# INFORMATION TO USERS

This manuscript has been reproduced from the microfilm master. UMI films the text directly from the original or copy submitted. Thus, some thesis and dissertation copies are in typewriter face, while others may be from any type of computer printer.

**The quality of this reproduction is dependent upon the quality of the copy submitted.** Broken or indistinct print, colored or poor quality illustrations and photographs, print bleedthrough, substandard margins, and improper alignment can adversely affect reproduction.

In the unlikely event that the author did not send UMI a complete manuscript and there are missing pages, these will be noted. Also, if unauthorized copyright material had to be removed, a note will indicate the deletion.

Oversize materials (e.g., maps, drawings, charts) are reproduced by sectioning the original, beginning at the upper left-hand corner and continuing from left to right in equal sections with small overlaps. Each original is also photographed in one exposure and is included in reduced form at the back of the book.

Photographs included in the original manuscript have been reproduced xerographically in this copy. Higher quality 6" x 9" black and white photographic prints are available for any photographs or illustrations appearing in this copy for an additional charge. Contact UMI directly to order.

**UMI**

A Bell & Howell Information Company
300 North Zeeb Road, Ann Arbor MI 48106-1346 USA
313/761-4700 800/521-0600

# POLARITON LOCAL STATES IN IMPURE CRYSTALS

by

VICTOR S. PODOLSKY

A dissertation submitted to the Graduate Faculty in Physics
in partial fulfillment of the requirements for the degree of
Doctor of Philosophy, The City University of New York

1998

This manuscript has been read and accepted for the Graduate Faculty in Physics in satisfaction of the dissertation requirement for the degree of Doctor of Philosophy.

04/24/98
Date

Chair of Examining Committee

4/28/98
Date

Executive Officer

Professor J. L. Birman

Professor A. Z. Genack

Professor P. Orland

Professor S. Schwartz

Supervisory Committee

THE CITY UNIVERSITY OF NEW YORK

# Abstract

POLARITON LOCAL STATES IN IMPURE CRYSTALS

by

Victor S. Podolsky

Adviser: Professor Alexander Lisyansky

We consider phonon-polariton local states in impure ionic crystals. Taking into account the defect-induced variations of the elastic constants, we found several local states of different symmetry. These states arise in the polariton gap for an infinitesimally small value of impurity strength, and they are predominated by long-wavelength modes. It is caused by the singularity in the density of the polariton states, which is generic for any isotropic dipole-active phonon mode with a negative dispersion. The crystal anisotropy removes this singularity and sets a finite threshold for local states. We investigate a crossover between polariton and phonon local states. We show that, due to a disproportion between the phonon and photon group velocities in 3D systems, the crossover takes place in a narrow spectral interval near the bottom of the gap, and the phonon content of the local states dominates over their photon content. To eliminate this disproportion, we place the active medium inside a narrow waveguide. We show that a coherent interaction between the waveguide modes and the polarization waves in an atomically thin dielectric layer (ionic 2D-crystal), gives rise to new excitations - 2D-polaritons. The features of their spectra and the structure of the defect-induced polariton local state depend on the waveguide width. When the width becomes comparable with the localization radius, 2D-polariton local state transforms into localized waveguide mode. Our estimates show that, in the sub-micron waveguides, the localized mode can be provided by a single impurity or a local structural defect.

# Acknowledgements

I wish to thank my advisor, Professor Lisyansky for providing guidance and support throughout all 4.5 years of my studies at Queens College.

I would like to thank Professor Deych for brining up the idea which gave the foundation of my current research. His expertise and critique were always a valuable help.

I am very fortunate to have love and support of my family. I am thankful to my wife and my son for all the patience and sacrifices they have made these past 4 years. I am indebted to my parents who put their faith in me.

I would like to thank all the Faculty and Staff of the Physics Department of Queens College for giving me an opportunity to come to New York and be a part of the Department, and I am thankful to my fellow graduate students who helped to make my life full and interesting.

This research was partially supported by a CUNY collaborative grant.

# Table of contents

# List of Illustrations

# Introduction

The theoretical and experimental investigation of photon localization is one of the most active areas in condensed matter physics. Originally, the search for this phenomenon was restricted to the strongly scattering disordered systems[1, 2, 3, 4, 5, 6, 7, 8]. The localization transition in this case must be accompanied by a drastic decrease in the photon diffusion coefficient and is expected to occure with increasing disorder. It can be achieved in dense systems of resonant scatterers, where the photon mean-free path and the scatterer size become comparable to the wavelength.

The possibility of photon localization in "impure photonic crystals", was proposed in Refs.[9, 10]. The photonic crystals present the artificially manufactured periodic dielectric systems, where propagating modes form separated bands. Inside the bandgaps, wave propagation is blocked by destructive interference between the Bragg-reflected waves. When the photonic crystal contains structural defects, these give rise to local photon states inside the bandgaps. However, it was soon realized that the 3-D photonic crystals with the gaps open in all directions are rather the exception than the rule [11]. Also, the intrinsic imperfectness of the man-made regular structures smears the band boundaries and additionally narrows the bandgaps.

The idea of exploiting local excitations in regular polar crystals and the concept of the polariton local states were introduced in Ref.[12]. The authors suggested that photons could be localized by means of their resonant interaction with local excitations. Considering a dipole-active impurity atom in an isotropic frequency-dispersive medium, authors discovered photon-atom bound states. These states describe an excited atom which is coherently coupled to the medium polaritons *via* the interaction with the electromagnetic field. If the intra-atom transition frequencies fall inside the

polariton gap, the radiative relaxation of the bound states is suppressed, and the induced field is localized around the impurity. The polariton-atom coupling was further analyzed in Ref.[13]. There it was shown that the two-level impurity model can be solved exactly by means of the Bethe-ansatz technique. The authors constructed a complete set of the scattering and bound states and analyzed the formation of the polariton-impurity band in a system of spatially correlated impurities.

A new development of the theory of the polariton local states was made in Ref.[14]. Considering a dipole-active medium with a point-like atomic defect (an isotope impurity, an "electronically rigid" impurity ion, etc.), the authors showed that *the spatial dispersion* of the medium has a surprisingly drastic effect on the local states, and discovered a new class of the polariton states. Among them, there are phonon-polariton states associated with the well-known phonon local states [15, 16]. The phonon states and their interaction with electromagnetic waves (IR absorption, Raman scattering) were extensively studied since the early forties following the pioneering work of I.M. Lifshitz [17]. In these studies, electromagnetic waves were considered as an external field which can scatter from the lattice and excite vibrational states. However, in ionic crystals, the resonant interaction between the lattice and the internal field (the photon-phonon crossing resonance) leads to the reconstruction of the optical phonon modes. In the cross-resonance region, the transverse-optical phonons and photons are coherently coupled and form new elementary excitations - polaritons. In a simple model of a crystal with a single dipole-active phonon mode, there are two polariton branches separated from each other by the spectral gap [18]. As was shown in Ref.[14], the lattice defects give rise to new local states inside the polariton gap. However, unlike for pure phonon local states, there is no lower critical value of the defect

strength that must be exceeded for the polariton local state to arise. It was found that this feature is caused by a negative dispersion of the optical phonons, resulting in non-monotonic polariton dispersion.

In this thesis, we explore the possibility of photon localization caused by the photon-phonon coupling in ionic crystals. In Chapter 1, we study the polariton local states in the isotropic dipole-active medium. The optical phonon excitations in this model are represented by two transverse branches and a single longitudinal branch. Such an approximation is appropriate when the long-wavelength dynamics of the cubic crystals is considered. In this approach, all details of the ion displacements within elementary cells are ignored and only resultant dipole moments of the cells are retained. It leaves the polarization and the electromagnetic fields as the only relevant dynamical variables.

We show that a single impurity embedded in the medium gives rise to local states inside the polariton gap. These states are composed from optical phonons and photons localized around the impurity. The spectral interval available for the local states is extended from the bottom of the polariton gap, $\Omega_{\max}^2$, to the bottom of the longitudinal band. These states arise at the bottom of the gap for an infinitesimally small value of the impurity strength. Our analysis shows that the states near $\Omega_{\max}^2$ are predominated by the long-wavelength polaritons. The typical momentum of these polaritons, $k_{\max}$, defines the coherence length of the local states, and the separation of the local states from the bottom of the gap, $\sqrt{\omega^2 - \Omega_{\max}^2}$, defines their localization radius. Despite the atomic size of a defect, both characteristic scales are macroscopic. These features of the local polariton states are caused by the singularity of the density of states at the bottom of the gap, $\rho_- (\omega^2) \propto (\Omega_{\max}^2 - \omega^2)^{-1/2}$, which is provided by

long-wavelength polaritons.

The local states drift away from the bottom of the gap with increasing impurity strength. This weakens the photon content of the polariton states and transforms them into the ordinary local phonon states. The long-wavelength nature of the states allows us to analyze this transition within the continuum approximation [19]. Our results show that the crossover takes place in a narrow interval near the bottom of the polariton gap. However, despite the small size of the crossover interval, the polariton resonance affects the selection of the defects allowing local states in the entire gap. In the case of isotopic defects, only light impurities can produce the local states in the "narrow" gaps.

In Chapter 2 we investigate the effects of the crystal symmetry on local states in cubic crystals. Considering a crystal with a defect which locally affects the elastic constants, we found two series of local states of different parity [20]. The even states resemble the ones considered within the dipole-active medium approximation in Chapter 1. Their frequencies depend on both deviation of the mass and deviation of the elastic constant in a defective cell. In contrast, the odd states depend on variations of the elastic constants only. The odd states correspond to "rhombic" and "tetragonal" oscillations localized around the stationary impurity. Among them, the "rhombic" states have the smallest separation from the bottom of the gap, which might indicate a dynamical structural instability of impure cubic crystals.

Local polariton states arise in the gap for an infinitesimally small value of the impurity strength. This absence of the lower threshold is due to the singularity in the density of the polariton states, which is generic for any isotropic parent phonon mode with negative dispersion. Introducing weak crystal anisotropy, we show that it

removes the singularity from the bottom of the gap, $\rho_-(\omega^2) \propto (\Omega_{\max}^2 - \omega^2 + A)^{-1/2}$, and sets a finite threshold for the local polariton states.

The local polariton states provide a "phonon assisted localization" of electromagnetic waves. However, our estimate of the energy partition shows that the phonon content of the local states greatly exceeds their photon content. It is caused by the fact that the cross-resonance momentum, $k_0$, is much smaller than the typical momentum of the modes dominating the local states, $k_{\max} \sim k_0 \beta^{-1/2}$, where $\beta = v/c$ is the ratio of the phonon velocity and the speed of light. To eliminate this disproportion, we place the active medium inside a narrow waveguide.

In Chapter 3, we investigate polarization waves in an atomically thin dielectric layer (ionic 2D-crystal) [21]. The layer is placed in a narrow parallel-plate waveguide. The coherent interaction between the waveguide modes and the polarization waves produces new excitations - 2D-polaritons. The stability of a regular 2D-crystal is provided by a strong confining potential, which also eliminates the activationless mode from the 2D-polariton spectrum. In such a system, the position of the maximum in the lower polariton branch depends on the waveguide width. We show that $k_{\max} \sim k_0$ when the waveguide width, $l$, is of the order of $\beta^{-2/3} a \sim 10^4 a$, and $k_{\max}$ approaches $\beta^{2/3} a^{-1}$ for $l \gg \beta^{-2/3} a$. In the later case, the frequency region of the polariton local states is enlarged by a factor $\beta^{-1/3} \sim 10^2$,compared to the 3D-case. We show that, due to the contribution from the upper polariton band, the electric field in these states is delocalized across the 2D-crystal within a distance of the order of $l$ from the defect. Upon increase of the impurity strength, the localization radius decreases, and the contributions to the field from the lower and upper branches begin to compete everywhere in the waveguide. When the localization length becomes comparable with

the waveguide width, the field is no longer confined near the dielectric layer and the polariton local state transforms into the localized waveguide mode. Our estimates show that, in the waveguide with $l \sim \beta^{-2/3} a$, localized modes can be produced by a single impurity or a local structural defect.

# 1. Impurity-induced local states in a dipole-active medium

In this chapter, we study properties of local polariton states and investigate the crossover between the polariton and phonon states within the continuum approximation.

## 1.1. Local polariton states

Let us consider a dipole-active medium with an embedded impurity. Dynamical equations of the medium can be introduced phenomenologically or derived from the microscopic equations. In the latter case, the displacements of ions within each cell must first be expressed *via* the dipole momentum of a cell, the displacement of its center of mass and other similar variables, then the continuum limit of the equations must be worked out. The resultant theory describes long-wavelength dynamics of a crystal where the electric field effectively interacts with the optical phonons only:

$$\left(\omega^2 - \hat{\Omega}^2\right) \mathcal{P}_{\mathbf{k}} = -\frac{d^2}{4\pi} \mathbf{E}_{\mathbf{k}} + \alpha \frac{a^3}{V} \mathcal{P}(0), \tag{1.1}$$

$$\left(\omega^2 - c^2 k^2\right) \mathbf{E}_{\mathbf{k}} = -4\pi \left[\left(\omega^2 - c^2 k^2\right) \hat{\mathbf{P}}_{\parallel} + \omega^2 \hat{\mathbf{P}}_{\perp}\right] \mathcal{P}_{\mathbf{k}}. \tag{1.2}$$

Here $\mathcal{P}_{\mathbf{k}}$ and $\mathbf{E}_{\mathbf{k}}$ are Fourier components of the polarization and electric fields, $\mathcal{P}(0)$ is the defect polarization, $\hat{\Omega}^2(\mathbf{k})$ is the dynamical matrix of the medium, $\hat{\mathbf{P}}_{\parallel}$ and $\hat{\mathbf{P}}_{\perp}$ are the longitudinal and the transverse projectors in the momentum space, $a$ is the lattice parameter, $V$ is the sample volume, and $d^2$ is the photon-phonon coupling parameter.

Eq.(1.1) implies that the defect is electrically identical with the replaced host ion. In this case the "defect strength" can be expressed as $\alpha = \omega'^2 \delta\nu/\nu - \omega^2 \delta\mu/\mu$, where $\mu$ and $\nu$ are the reduced mass of the elementary cell and the elastic constant of the

nearest-neighbor bonds, $\delta\mu$, $\delta\nu$ are their impurity-induced variations, and $\omega'^2$ is a characteristic frequency dependent on the properties of a defect in the crystal.

In the isotropic medium the dynamical matrix can be presented as follows:

$$\hat{\mathbf{\Omega}}^2 = \Omega_{\|}^2 \hat{\mathbf{P}}_{\|} + \Omega_{\perp}^2 \hat{\mathbf{P}}_{\perp}, \tag{1.3}$$

where $\Omega_{\|}^2$ and $\Omega_{\perp}^2$ are the frequencies of the longitudinal and the transverse-optical phonons. We assume a negative dispersion in the phonon branches, and use the standard long-wavelength asymptotes:

$$\Omega_{\perp}^2(k) \approx \Omega_0^2 - v_{\perp}^2 k^2, \tag{1.4}$$

$$\Omega_{\|}^2(k) \approx \Omega_0^2 - v_{\|}^2 k^2, \tag{1.4'}$$

where the parameters $v_{\perp}$ and $v_{\|}$ set the ranges of the typical phonon velocities, and due to isotropy of the system both branches have the same activation frequency, $\Omega_0$. For the "order of magnitude" estimates we assume $v_{\perp} \sim v_{\|} \sim 10^2$m/s, and $\Omega_0 \sim v/a \sim d$.

Solving Eqs.(1.1-1.3), one can express $\mathbf{E_k}$ and $\mathcal{P}_\mathbf{k}$ in terms of the defect polarization, $\mathcal{P}(\mathbf{0})$, and then obtain the spectral equation:

$$1 = \frac{\alpha}{3}\left(\frac{a}{2\pi}\right)^3 \int d\mathbf{k} \left[ \left(\omega^2 - \Omega_{\|}^2 - d^2\right)^{-1} + 2\left(\omega^2 - \Omega_{\perp}^2 - \frac{d^2\omega^2}{\omega^2 - c^2k^2}\right)^{-1} \right] = \alpha\, I(\omega^2). \tag{1.5}$$

This equation defines spectra of all, extended and local, excitations. The extended states form continuous bands and their dispersion relations are determined by the poles of the integrand in Eq.(1.5). In our model there is a single longitudinal branch, $\omega^2 = \Omega_{\|}^2 + d^2$, whereas the transverse band contains two polariton branches [Fig.1]:

$$\Omega_{\pm}(k) = \frac{1}{2}\left[\sqrt{(\Omega_{\perp} + ck)^2 + d^2} \pm \sqrt{(\Omega_{\perp} - ck)^2 + d^2}\right]. \tag{1.6}$$

The lower branch is activationless and non-monotonic. Analysis of its "large-momenta" asymptote,

$$\Omega_{-}^{2} \approx \Omega_{\perp}^{2}\left(1-\frac{d^{2}}{c^{2}k^{2}}\right), \tag{1.7}$$

shows that the lower branch reaches its maximum at the point

$$k_{\max} \approx \left(\frac{2d\Omega_{0}}{v_{\perp}c}\right)^{1/2} \sim \beta^{1/2}a^{-1}, \tag{1.8}$$

where $\beta = v/c$ is a small parameter. Since $vk_{\max} \sim \beta^{1/2}\Omega_0 \ll \Omega_0$, and $ck_{\max} \sim \beta^{-1/2}\Omega_0 \gg \Omega_0$, the maximum of $\Omega_{-}^{2}(k)$ is located in the long-wavelength region but far away from the cross-resonance point. Using Eqs.(1.7-1.8) one can evaluate:

$$\Omega_{\max}^{2} = \Omega_{0}^{2} - \Delta_{1} \approx \Omega_{0}^{2} - 2\beta d\Omega_{0}. \tag{1.9}$$

The upper polariton branch $\Omega_{+}^{2}(k)$ has a positive slope and a non-zero activation frequency $\Omega_{+}^{2}(0) = \Omega_{0}^{2}+d^{2}$. Therefore, the polariton branches are separated by the gap extended from $\Omega_{\max}^{2}$ to $\Omega_{0}^{2}+d^{2}$. However, because the longitudinal branch overlaps the top part of the polariton gap, the true spectral gap is between $\Omega_{\max}^{2}$ and the minimum of the longitudinal branch, $\Omega_{\min}^{2} = \Omega_{0}^{2}+d^{2}-\Delta_{\|}$. The spectral gap is open only if the width of the polariton gap, $d^{2}+\Delta_{1}$, exceeds the width of the longitudinal band $\Delta_{\|}$. Further below we assume this and consider only the local states inside the gap.

The frequency of the local state can be found from Eq.(1.5). The integral $I(\omega^{2})$ in this equation presents a sum of the "longitudinal" and "transverse" terms, $I_{\|}(\omega^{2})$ and $I_{\perp}(\omega^{2})$. The transverse integral can be written in the form:

$$I_{\perp}(\omega^{2}) = \frac{2}{3}\left(\frac{a}{2\pi}\right)^{3}\int d\mathbf{k}\frac{\omega^{2}-c^{2}k^{2}}{\left(\omega^{2}-\Omega_{+}^{2}\right)\left(\omega^{2}-\Omega_{-}^{2}\right)}. \tag{1.10}$$

When the frequency approaches $\Omega_{\max}$, this integral diverges at the surface $\mathbf{k}^{2} = k_{\max}^{2}$. Near the bottom of the gap ($\omega \gtrsim \Omega_{\max}$) the transverse term dominates in $I(\omega^{2})$ and

the region of $k \sim k_{\max}$ gives the major contribution to $I_\perp(\omega^2)$. As it follows from Eqs.(1.6-1.9), in this region we can approximate:

$$\Omega_-^2 \approx \Omega_{\max}^2 - 4v_\perp^2 \, (k - k_{\max})^2 . \tag{1.11}$$

$$\Omega_-^2 \approx \Omega_0^2 + d^2 - c^2 k^2 . \tag{1.11'}$$

what allows us to evaluate $I(\omega^2)$ in Eq.(1.5) and find the frequency of the local state:

$$\sqrt{\omega^2 - \Omega_{\max}^2} \approx \frac{\alpha \, a}{3\pi \, v_\perp} \, (a \, k_{\max})^2 \sim \alpha \, \beta \, \Omega_0^{-1} . \tag{1.12}$$

This result shows that the local polariton state arises at the bottom of the gap for an infinitesimally small defect strength ($\alpha \gtrsim +0$). To evaluate the localization radius of this state we need to consider the spatial distribution of the electric and the polarization fields. Using the solution of Eqs.(1.1-1.2), we obtain:

$$\mathbf{E}\,(\mathbf{r}) = -\frac{\alpha \, a^3}{2\,\pi^2} \int d\mathbf{k} \, \exp\,(i\mathbf{k}\mathbf{r}) \left[ \frac{\hat{\mathbf{P}}_\parallel}{\omega^2 - \Omega_\parallel^2 - d^2} + \frac{\omega^2 \, \hat{\mathbf{P}}_\perp}{(\omega^2 - \Omega_-^2)\,(\omega^2 - \Omega_-^2)} \right] \mathcal{P}(0). \tag{1.13}$$

Near the bottom of the gap the longitudinal part is small comparing to the transverse field. Taking into account that the region of $k \sim k_{\max}$ gives the main contribution to $\mathbf{E}_\perp\,(\mathbf{r})$ and employing Eqs.(1.11-1.12), one can evaluate:

$$\mathbf{E}_\perp\,(\mathbf{r}) \approx 4\pi \frac{\Omega_0^2}{c^2 k_{\max}^2} \, \{\mathbf{n} \times [\mathbf{n} \times \mathcal{P}(0)]\} \, \frac{\sin\,(r k_{\max}) \exp\,(-r\varkappa)}{r k_{\max}} . \tag{1.14}$$

In a similar way one can obtain:

$$\mathcal{P}_\perp(\mathbf{r}) \approx \{\mathbf{n} \times [\mathbf{n} \times \mathcal{P}(0)]\} \, \frac{\sin\,(r k_{\max}) \exp\,(-r\varkappa)}{r k_{\max}} , \tag{1.15}$$

where $\mathbf{n}$ is the unit radial vector, and

$$\varkappa = \sqrt{\frac{\omega^2 - \Omega_{\max}^2}{4v_\perp^2}} \approx \frac{\alpha a}{6\pi v_\perp^2} \, (a k_{\max})^2 \sim a^{-1} \beta \, \frac{\alpha}{\Omega_0^2} \tag{1.16}$$

is the inverse localization radius of the considered state.

Equations (1.14-1.15) allow us to estimate the energy partition between the phonons and photons bound in the local state. Taking into account that the polarization and the electric fields are concentrated within the $\varkappa^{-1}$-range from the defect, we can evaluate their energies as follows:

$$W_{\text{mech}} \sim \int \mathcal{P}^2(\mathbf{r})d\mathbf{r} \sim \mathcal{P}^2(0)\ k_{\max}^{-2}\varkappa^{-1}, \tag{1.17}$$

$$W_{\text{field}} \sim \int \mathbf{E}^2(\mathbf{r})d\mathbf{r} \sim \mathcal{P}^2(0)\ \left(\frac{\Omega_0}{c\,k_{\max}}\right)^4 k_{\max}^{-2}\varkappa^{-1}. \tag{1.17'}$$

It gives us the "order of the magnitude" estimate of the ratio of two energies:

$$\frac{W_{\text{field}}}{W_{\text{mech}}} \sim \left(\frac{\Omega_0}{c\,k_{\max}}\right)^4 \sim \beta^2 \tag{1.18}$$

The features of the polariton states near the bottom of the gap is caused by the specifics of the density of states in the lower polariton band. Since $\Omega_-^2(k)$ reaches its maximum at the surface of a finite area inside the Brillouin zone, the density of states in the lower polariton band diverges at the bottom of the gap. Its leading term can be calculated with the help of Eq.(1.11):

$$\rho\left(\omega^2\right) = \left(\frac{a}{2\pi}\right)^3 \oint_{\Omega_-=\omega} d\sigma \left[\frac{d\Omega_-^2(k)}{dk}\right]^{-1} \approx \frac{a\ (ak_{\max})^2}{(2\pi)^2\ v_\perp\ \sqrt{\Omega_{\max}^2 - \omega^2}} \tag{1.19}$$

This singularity is provided by the long-wavelength polaritons ($k \sim k_{\max}$) ,which also dominate in the local states near the bottom of the gap. It explains the macroscopic size of the coherence length, $l_{\text{coh}} \sim k_{\max}^{-1}$, and localization radius, $l_{\text{loc}} \sim \varkappa^{-1}$. On the other hand, because the typical momentum of these modes is far away from the cross-resonance point ($k_{\max} \gg k_0$), the phonon content of the local states greatly exceeds their photon content. The frequency range, where these states can be described by

Eqs.(1.12-1.15), is the interval where the square-root singularity dominates in the density of states. Setting $\rho(\omega^2) \gg \Delta^{-1}$,where $\Delta$ is the width of the lower polariton band, one can be estimate:

$$\sqrt{|\Omega_{\max}^2 - \omega^2|} \ll \frac{a\,\Omega_{\max}^2\,(ak_{\max})^2}{(2\pi)^2\ v_\perp} \sim \beta\,\Omega_0. \tag{1.20}$$

The local polariton states appear first at the bottom of the gap for $\alpha = +0$ and move inside the gap upon increase of the defect strength. When $\alpha \ll \Omega_{\max}^2$ the local states lie in the immediate vicinity of $\Omega_{\max}^2$. Further increase of $\alpha$ drives them away from the bottom of the gap what weakens the photon content of the local states and transforms them into the ordinary phonon states.

## 1.2. Crossover between the polariton and phonon local states

To investigate the crossover between the polariton and phonon local states we need to analyze Eqs.(1.1-1.2, 1.5) in the entire spectral gap. Away from the bottom of the gap both terms of Eq.(1.5), $I_\parallel(\omega^2)$ and $I_\perp(\omega^2)$, become comparable and calculations here require knowledge of the phonon dispersion relations in the entire Brillouin zone. Such detailed information is not consistent with the approximations employed in our model. In the short-wavelength region a crystal anisotropy cannot be neglected, and ion displacements within elementary cells must be considered in all details. However, assuming that the crossover takes place near the bottom of the gap, we proceed with calculations noting that in the isotropic model it is sufficient to know only the densities of states in the phonon bands. We use a simple approximation accounting only for Kohn's singularities at the band boundaries:

$$\rho_{\text{phon}}(\varepsilon) = \frac{8}{\pi\,\Delta_{\text{phon}}^2}\sqrt{(\varepsilon - \omega_{\min}^2)\,(\omega_{\max}^2 - \varepsilon)}, \tag{1.21}$$

where $\Delta_{\rm phon}$ is the width of the phonon band; $\omega^2_{\rm min}$ and $\omega^2_{\rm max}$ are the band boundaries.

To calculate $I_{\|}(\omega^2)$ we transform it into the integral over the longitudinal band:

$$I_{\|}(\omega^2) = \frac{1}{3}\left(\frac{a}{2\pi}\right)^3 \int \frac{d\mathbf{k}}{\omega^2 - \Omega^2_{\|} - d^2} = \frac{1}{3}\int_{\Omega^2_{\rm min}}^{\Omega^2_{\rm min}+\Delta_{\|}} \frac{\rho_{\|}(\varepsilon)\,d\varepsilon}{\omega^2 - \varepsilon}. \qquad (1.22)$$

where $\Omega^2_{\rm min} = \Omega^2_0 + d^2 - \Delta_{\|}$. Using here Eq.(1.21) for $\rho_{\|}(\varepsilon)$ one can obtain:

$$I_{\|}(\omega^2) = -\frac{4}{3\Delta^2_{\|}}\left(\sqrt{\Omega^2_{\rm min} + \Delta_{\|} - \omega^2} - \sqrt{\Omega^2_{\rm min} - \omega^2}\right)^2. \qquad (1.23)$$

To evaluate the transverse integral we present it as a sum of two terms by separating the Brillouin zone into two parts:

$$I_{\perp}(\omega^2) = \frac{2}{3}\left(\frac{a}{2\pi}\right)^3 \int d\mathbf{k}\left(\omega^2 - \Omega^2_{\perp} - \frac{d^2\omega^2}{\omega^2 - c^2k^2}\right)^{-1} = I'_{\perp}(\omega^2) + I''_{\perp}(\omega^2). \qquad (1.24)$$

The first term, $I'_{\perp}(\omega^2)$, involves integration over $k < k'_0$ including the cross-resonance region, and $I''_{\perp}(\omega^2)$ presents the integral over the remaining part of the Brillouin zone, $k > k'_0$. The separating momentum $k'_0$ is convenient to fix by the condition $\Omega^2_{\perp}(k'_0) = \Omega^2_{\rm max}$ [Fig.1].

Since $k'_0$ is located far away from the cross-resonance point, the product $ck$ in $I''_{\perp}(\omega^2)$ greatly exceeds the typical phonon frequencies and there we can set $ck = \infty$:

$$I''_{\perp}(\omega^2) \approx \frac{2}{3}\left(\frac{a}{2\pi}\right)^3 \int_{k>k'_1} \frac{d\mathbf{k}}{\omega^2 - \Omega^2_{\perp}} = \frac{2}{3}\int_{\Omega^2_0 - \Delta_{\perp}}^{\Omega^2_{\rm max}} \frac{\rho_{\perp}(\varepsilon)\,d\varepsilon}{\omega^2 - \varepsilon}. \qquad (1.25)$$

Using now Eq.(1.21) for $\rho_{\perp}(\varepsilon)$, one can calculate the last integral:

$$I''_{\perp}(\omega^2) = \frac{16}{3\pi\Delta_{\perp}}\left[(2\delta - 1)\arcsin\sqrt{\delta_1} - \sqrt{\delta_1(1-\delta_1)} + \sqrt{\delta\,|1-\delta|}\,F(\omega^2)\right], \qquad (1.26)$$

where

$$F(\omega^2) = \begin{cases} +\ln\dfrac{\sqrt{\delta(1-\delta_1)} + \sqrt{\delta_1(1-\delta)}}{\sqrt{\delta(1-\delta_1)} - \sqrt{\delta_1(1-\delta)}} & \text{for } \Omega^2_{\rm max} \le \omega^2 \le \Omega^2_0, \\ -2\arctan\sqrt{\dfrac{\delta_1(\delta-1)}{\delta(1-\delta_1)}} & \text{for } \omega^2 \ge \Omega^2_0. \end{cases} \qquad (1.27)$$

and we denote $\delta_1 = (\Delta_\perp - \Delta_1)\,/\,\Delta_\perp$, and $\delta = (\Delta_\perp + \omega^2 - \Omega_0^2)\,/\,\Delta_\perp$.

Considering $\omega^2$ far away from the bottom of the gap ($\omega^2 - \Omega_{\max}^2 \gg \Delta_1$), one can obtain:

$$I''_\perp(\omega^2) \approx \frac{8}{3\,\Delta_\perp^2}\left(\sqrt{\omega^2 + \Delta_\perp - \Omega_0^2} - \sqrt{\omega^2 - \Omega_0^2}\right)^2. \tag{1.28}$$

In the opposite limit, $\omega \to \Omega_{\max}$, Eqs.(1.26-1.27) lead to the logarithmic singularity:

$$I''_\perp(\omega^2) \propto -\frac{16\,\Delta_1^{1/2}}{3\,\pi\,\Delta_\perp^{3/2}} \ln\frac{\omega^2 - \Omega_{\max}^2}{\Delta_\perp}. \tag{1.29}$$

The second term in Eq.(1.24) includes the integration over the cross-resonance region where the polariton effect cannot be neglected. It leaves $I'_\perp(\omega^2)$ in the form:

$$I'_\perp(\omega^2) = -\frac{2}{3}\int_{\Omega_{\max}^2}^{\Omega_0^2} \frac{(\omega^2 - c^2k^2)\,\rho_\perp(\varepsilon)\,d\varepsilon}{(\omega^2 - c^2k^2)\,(\varepsilon - \omega^2) + d^2\omega^2}. \tag{1.30}$$

Recalling that $I'_\perp(\omega^2)$ presents the integral over the long-wavelength domain and using Eq.(1.21), we can present $I'_\perp(\omega^2)$ as follows:

$$I'_\perp(\omega^2) = \frac{16\Delta_1}{3\pi\Delta_\perp^2}\int_0^1 \frac{x^{3/2}\,(b-x)^{1/2}\,dx}{(x-a_+)\,(x-a_-)}. \tag{1.31}$$

Here $b{=}\Delta_\perp/\Delta_1$ is a large parameter and two poles of the integrand are given by the equation:

$$a_\pm = \frac{1}{2\Delta_1}\left[\,\Omega_0^2 - \omega^2 \pm \left(\omega^2 - \omega_-^2\right)^{1/2}\left(\omega^2 - \omega_-^2\right)^{1/2}\right], \tag{1.32}$$

where $\omega_\pm^2 = \Omega_0^2 \pm \Delta_1$, so that $\omega_-^2$ coincides with the gap's bottom, $\Omega_{\max}^2$.

Within the range, $\omega_-^2 \le \omega^2 \le \omega_+^2$, where $a_+$ and $a_-$ are complex, $I'_\perp(\omega^2)$ has the form:

$$\begin{aligned} I'_\perp(\omega^2) \;=\; & \frac{16\Delta_1^{1/2}}{3\pi\Delta_\perp^{3/2}}\left[2 + \frac{\nu^2 - 3\eta^2}{2\eta}\left(\arctan\frac{1-\nu}{\eta} + \arctan\frac{1+\nu}{\eta}\right)\right. \\ & \left. + \frac{3\nu^2 - \eta^2}{4\nu}\ln\frac{(1-\nu)^2 + \eta^2}{(1+\nu)^2 + \eta^2}\right], \end{aligned} \tag{1.33}$$

where the parameters $\nu$ and $\eta$ are defined by the equations:

$$\nu^2 - \eta^2 = \frac{\Omega_0^2 - \omega^2}{2\Delta_1}, \tag{1.34}$$

$$2\nu\eta = \frac{\left(\omega_-^2 - \omega^2\right)^{1/2}\left(\omega^2 - \omega_-^2\right)^{1/2}}{2\Delta_1}. \tag{1.34'}$$

One can check that, in agreement with the previously obtained results, Eqs.(1.33-34') give the square-root singularity of $I'_\perp(\omega^2)$ at the bottom of the gap:

$$I'_\perp(\omega^2) \propto \frac{8\Delta_1}{3\Delta_\perp^{3/2}}\left(\omega^2 - \Omega_{\max}^2\right)^{-1/2}. \tag{1.35}$$

For $\omega^2 \geq \Omega_0^2 + \Delta_1$, when $a_\pm$ have real negative values, we obtain:

$$I'_\perp(\omega^2) = \frac{32\Delta_1^{1/2}}{3\pi\Delta_\perp^{3/2}}\left(1 - \frac{|a_-|^{3/2}\arctan|a_-|^{-1/2} - |a_-|^{3/2}\arctan|a_-|^{-1/2}}{|a_-| - |a_-|}\right). \tag{1.36}$$

At the upper boundary of the gap, assuming $d^2 - \Delta_\parallel \gg \Delta_1$, Eqs.(1.33-34') give us:

$$I'_\perp(\Omega_{\min}^2) \approx \left(\frac{\Delta_1}{\Delta_\perp}\right)^{3/2}\frac{32}{9\pi\left(d^2 - \Delta_\parallel\right)}. \tag{1.37}$$

Eqs.(1.23, 1.26-27, 1.33-34') allow us to analyze the local states in the entire gap. Since any local state presents a superposition of all normal modes, we can qualitatively describe its composition comparing contributions to $I(\omega^2)$ from different bands.

As we showed, the function $I(\omega^2)$ has the singularity at the bottom of the gap caused by the long-wavelength polaritons. They also give the major contribution to $I(\omega^2)$ inside the narrow interval, $\Omega_{\max}^2 < \omega^2 \ll \Omega_{\max}^2 + \Delta_1$. The structure of a state from this region shows directly that it is formed from the polaritons with $k \sim k_{\max}$. However, even for $\omega^2 = \Omega_0^2$, their contribution to $I(\omega^2)$ is substantially weakened. From Eqs.(1.26-27, 1.33-34') we obtain:

$$I_\perp(\Omega_0^2) = \frac{8}{3\Delta_\perp}\left[1 + \mathcal{O}\left(\sqrt{\frac{\Delta_1}{\Delta_\perp}}\right)\right], \tag{1.38}$$

where the leading term is provided by the short-wavelength ($k > k_0'$) polaritons, which are physically indistinguishable from the transverse-optical phonons.

Outside the interval $\Omega_{\max}^2 \leq \omega^2 \leq \Omega_{\max}^2 + 2\Delta_1$, function $I(\omega^2)$ has basically the phonon structure. The long-wavelength polariton contribution is there weakened by the power factors of the small ratio, $\Delta_1/\Delta_\perp$. At the upper boundary of the gap, Eqs.(1.23, 1.28, 1.37) give us:

$$I(\Omega_{\min}^2) = \frac{8}{3\Delta_\parallel^2}\left[\left(\frac{\sqrt{x+y}-\sqrt{y}}{x}\right)^2 - \frac{1}{2}\right] + \mathcal{O}\left(\sqrt{\frac{\Delta_1}{\Delta_\perp}}\right), \tag{1.39}$$

where $x = \Delta_\perp/\Delta_\parallel$ and $y = d^2/\Delta_\parallel - 1$.

$I(\Omega_{\min}^2)$ determines the upper limit of the impurity strength, which allows the local states. Its value can be positive or negative depending on the relations between the ion plasma frequency $d^2$ and the widths of phonon bands $\Delta_\perp$ and $\Delta_\parallel$. Eq.(1.39) shows that $I(\Omega_{\min}^2)$ is positive only if the width of the spectral gap does not exceed a certain value,

$$d^2 - \Delta_\parallel \leq (\Delta_\parallel/8)\left(2 - \Delta_\perp/\Delta_\parallel\right)^2. \tag{1.40}$$

Therefore, only in "narrow" gaps all local states are associated with impurities of the same type. In the case of isotope defects, for instance, the local polariton states arise only in the presence of light impurities. However, if $d^2 - \Delta_\parallel$ exceeds the critical value, the local states near the top and the bottom of the gap are associated with different types of defects. For isotopes these are heavy and light impurities, respectively. The frequency regions of the corresponding states are limited inside the gap. The upper frequency for the "light" states and lower frequency for the "heavy" ones can be found from the equations, $\omega^2 I(\omega^2) = 1$ and $I(\omega^2) = 0$, respectively.

# 2. Local states in the cubic crystals

The analysis of the local polariton states made in the previous chapter does not take into account the regular microscopic structure of ionic crystals. The only lattice effects we have accounted for were a finite size of the Brillouin zone and finite widths of the phonon bands. Since the properties of the polariton states critically depend on the symmetry of the long-wavelength asymptotes of the phonon spectra, we can suggest that the model of the isotropic dipole-active medium presents a "zero-order" approximation of a cubic crystal. In this chapter we analyze the effects of the lattice symmetry on the local polariton states in cubic crystals.

## 2.1. Lattice dynamics in the isotropic approximation

Let us consider a body centered cubic (BCC) crystal with two oppositely charged ions per each elementary cell [Fig.2]. Denoting masses of the positive and negative ions as $m_+$ and $m_-$, respectively, and their displacements as $\mathbf{U}_\pm(\mathbf{r})$, where $\mathbf{r}$ belongs to the positive or negative sublattice; we can write down the equations of the stationary lattice excitations coupled with the coherent electric field $\mathbf{E}(\mathbf{r})$:

$$m_\pm\omega^2\mathbf{U}_\pm(\mathbf{r}) \pm q\mathbf{E}(\mathbf{r}) = -\sum_s \left[\sum_{\mathbf{R}_s} \mathbf{f}\left(\mathbf{r},\mathbf{R}_s\right) + \sum_{\mathbf{R}'_s} \mathbf{f}'\left(\mathbf{r},\mathbf{R}'_s\right)\right], \qquad (2.1)$$

where $q$ denotes an ion charge, and $\omega$ is the frequency.

The right-hand side of Eq.(2.1) presents all elastic forces acting on the ion hosted at the site $\mathbf{r}$. Vectors $\mathbf{R}_s$ and $\mathbf{R}'_s$ denote radius-vectors of ions in the $s^{\text{th}}$-neighboring shells of the original and alternative sublattice, respectively. Assuming a central interaction between ions, we present the elastic forces within one sublattice in the

form:

$$\mathbf{f}(\mathbf{r},\mathbf{R}_s) = -\frac{\gamma(R_s)}{R_s^2}\mathbf{R}_s\left\{\mathbf{R}_s\cdot\left[\mathbf{U}_{\pm}(\mathbf{r})-\mathbf{U}_{\pm}(\mathbf{r}+\mathbf{R}_s)\right]\right\}, \tag{2.2}$$

and the forces between ions from different sublattices are:

$$\mathbf{f}'\left(\mathbf{r},\mathbf{R}_s'\right) = -\frac{\gamma'(R_s')}{R_s'^2}\mathbf{R}_s'\left\{\mathbf{R}_s'\cdot\left[\mathbf{U}_{\pm}(\mathbf{r})-\mathbf{U}_{\mp}(\mathbf{r}+\mathbf{R}_s')\right]\right\}, \tag{2.2'}$$

where the intensities of the intra- and inter-sublattice interactions, $\gamma(R)$ and $\gamma'(R')$, depend on the distance between ions only.

The coherent electric field induced by the ionic vibrations, $\mathbf{E}(\mathbf{r})$, invokes an additional pair of equations:

$$\nabla\cdot\mathbf{E}(\mathbf{r}) = -4\pi q\sum_{\mathbf{l}}\left[\mathbf{U}_{+}(\mathbf{l})\cdot\nabla\delta(\mathbf{r}-\mathbf{l})-\mathbf{U}_{-}(\mathbf{l}')\cdot\nabla\delta(\mathbf{r}-\mathbf{l}')\right]. \tag{2.3}$$

$$\nabla\times\left[\nabla\times\mathbf{E}(\mathbf{r})\right]+\frac{\omega^2}{c^2}\mathbf{E}(\mathbf{r}) = -\frac{4\pi q\omega^2}{c^2}\sum_{\mathbf{l}}\left[\mathbf{U}_{+}(\mathbf{l})\,\delta(\mathbf{r}-\mathbf{l})-\mathbf{U}_{-}\left(\mathbf{l}'\right)\,\delta(\mathbf{r}-\mathbf{l}')\right], \tag{2.4}$$

where $\mathbf{l}$ and $\mathbf{l}' = \mathbf{l}+\mathbf{b}$ denote the lattice vectors,and $\mathbf{b}$ is the basis vector.

The lattice normal modes arise as simultaneous solutions of Eqs.(2.1-4). Fourier transformation of this system gives the dynamical equation in the momentum representation:

$$\begin{pmatrix} \hat{\mathbf{D}}(\mathbf{k})+\hat{\mathbf{F}}(\mathbf{k})-\omega^2 m_- & \hat{\mathbf{D}}'(\mathbf{k})-\hat{\mathbf{F}}(\mathbf{k}) \\ \hat{\mathbf{D}}'(\mathbf{k})-\hat{\mathbf{F}}(\mathbf{k}) & \hat{\mathbf{D}}(\mathbf{k})+\hat{\mathbf{F}}(\mathbf{k})-\omega^2 m_- \end{pmatrix}\begin{pmatrix} \mathbf{A}_-(\mathbf{k}) \\ \mathbf{A}_-(\mathbf{k}) \end{pmatrix} = 0. \tag{2.5}$$

Here $\mathbf{A}_{\pm}(\mathbf{k})$ denote the Fourier amplitudes of the displacements, $\hat{\mathbf{D}}(\mathbf{k})$ is the dynamical matrix of the intra-sublattice interaction:

$$\hat{\mathbf{D}}(\mathbf{k}) = \sum_s\frac{\gamma(R_s)}{R_s^2}\sum_{\mathbf{R}_s}\mathbf{R}_s\otimes\mathbf{R}_s\left[1-\exp(i\mathbf{k}\mathbf{R}_s)\right]+\frac{\gamma'(R_s')}{R_s'^2}\sum_{\mathbf{R}_s'}\mathbf{R}_s'\otimes\mathbf{R}_s', \tag{2.6}$$

and $\hat{\mathbf{D}}'(\mathbf{k})$ is the dynamical matrix of the inter-sublattice interaction:

$$\hat{\mathbf{D}}'(\mathbf{k}) = -\sum_s \frac{\gamma'(R'_s)}{R'^2_s} \sum_{\mathbf{R}'_s} \mathbf{R}'_s \otimes \mathbf{R}'_s \exp\left(i\mathbf{k}\mathbf{R}'_s\right), \tag{2.6'}$$

where $\mathbf{R} \otimes \mathbf{R}$ denotes the direct product of two vectors, and operator $\hat{\mathbf{F}}(\mathbf{k})$ is defined as follows:

$$\hat{\mathbf{F}}(\mathbf{k}) = \frac{4\pi q^2}{a^3}\left(\hat{\mathbf{P}}_{\|} + \frac{\omega^2}{\omega^2 - c^2k^2}\hat{\mathbf{P}}_{\perp}\right). \tag{2.7}$$

The electric field can be expressed *via* the ion amplitudes:

$$\mathbf{E}(\mathbf{k}) = -\frac{\hat{\mathbf{F}}\left[\mathbf{A}_{-}(\mathbf{k}) - \mathbf{A}_{-}(\mathbf{k})\right]}{q}. \tag{2.8}$$

The dynamical matrices given by Eqs.(2.6-.6') are of a general type and solutions of Eq.(2.5), in general, do not split into the longitudinal and transverse modes. This takes place only in the isotropic approximation, which describes the long-wavelength dynamics of the cubic crystals. The isotropic parts of the dynamical matrices are provided by the long-range ($R, R' \gg a$) forces, as it can be seen from their structure:

$$\mathbf{D}^{\alpha\beta}(\mathbf{k})\big|_{\text{long-range}} \propto \sum_s \gamma(R_s)\big|_{(R_s \gg a)} \sum_{\mathbf{R}_s} R_s^{\alpha} R_s^{\beta} \left\{1, \exp\left(i\mathbf{k}\mathbf{R}_s\right)\right\} \approx$$

$$\int \gamma(R)\, 4\pi R^2 dR \int d\hat{\mathbf{R}} R^{\alpha} R^{\beta} \left\{1, \exp\left(i\mathbf{k}\mathbf{R}_s\right)\right\} \propto \left\{\delta^{\alpha\beta}, \frac{k^{\alpha}k^{\beta}}{k^2}\right\}. \tag{2.9}$$

Assuming that the intensity of the interaction, $\gamma(R)$, decreases slow enough with the distance between ions, and considering the long-wavelength lattice excitations in a weakly anisotropic crystal we can employ the isotropic approximation of the dynamical matrices in the entire Brillouin zone:

$$\hat{\mathbf{D}}(\mathbf{k}) = \gamma_{\|}(k)\hat{\mathbf{P}}_{\|} + \gamma_{\perp}(k)\hat{\mathbf{P}}_{\perp}, \tag{2.10}$$

$$\hat{\mathbf{D}}'(\mathbf{k}) = \gamma'_{\|}(k)\hat{\mathbf{P}}_{\|} + \gamma'_{\perp}(k)\hat{\mathbf{P}}_{\perp}, \tag{2.10'}$$

where the scalar functions $\gamma_\sigma(k)$ and $\gamma'_\sigma(k)$ can be expressed in terms of the frequencies of the longitudinal and transverse phonons.

In the crystals of the cubic symmetry, the dynamical matrices become trivial at the center of the Brillouin zone:

$$\hat{\mathbf{D}}(0) = -\hat{\mathbf{D}}'(0) = \sum_s \frac{\gamma'(R'_s)}{R'^2_s} \sum_{\mathbf{R}'_s} \mathbf{R}'_s \otimes \mathbf{R}'_s = \frac{1}{3} \sum_s \gamma'(R'_s)\, Z'_s = \gamma, \qquad (2.11)$$

where $Z'_s$ denotes a total number of ions in the $s^{\text{th}}$-shell. Due to this condition all $\gamma_\sigma(0)$ and $-\gamma'_\sigma(0)$ are equal to the same positive constant $\gamma$.

In the isotopic approximation, all normal modes of the crystal are either longitudinal or transverse, $\mathbf{A}^\sigma_\pm(\mathbf{k}) = \mathbf{e}_\sigma(\mathbf{k})\, A^\sigma_\pm(\mathbf{k})$, where $\mathbf{e}_\sigma(\mathbf{k})$ are the longitudinal or transverse unit polarization vectors, $\sigma$ is the polarization index. Eqs.(2.5, 2.10-10′) lead to the following relationship between the ion displacements in different sublattices:

$$A^{(\sigma)}_- = \frac{f_\sigma - \gamma'_\sigma}{\gamma_\sigma + f_\sigma - \omega^2 m_+}\, A^{(\sigma)}_-, \qquad (2.12)$$

where the parameter $f_\sigma$ depends on the polarization.

For the longitudinal modes $f_\parallel = \mu d^2$, where $\mu$ is the reduced mass of the elementary cell and $d^2 = 4\pi q^2/\mu a^3$ is the " ion plasma frequency". The corresponding dispersion equation,

$$\left(\frac{\gamma_\parallel + f_\parallel}{m_+} - \omega^2\right)\left(\frac{\gamma_\parallel + f_\parallel}{m_-} - \omega^2\right) - \frac{\left(\gamma'_\parallel - f_\parallel\right)^2}{m_+ m_-} = \left(\omega^2 - \omega^2_\parallel\right)\left(\omega^2 - \Omega^2_\parallel - d^2\right) = 0, \qquad (2.13)$$

defines the acoustic $\left(\omega^2_\parallel\right)$ and optical $\left(\Omega^2_\parallel\right)$ branches of the longitudinal phonons.

For the transverse modes

$$f_\perp = \frac{\mu d^2 \omega^2}{\omega^2 - c^2 k^2}, \qquad (2.14)$$

therefore, their dispersion equation,

$$\left(\frac{\gamma_\perp + f_\perp}{m_+} - \omega^2\right)\left(\frac{\gamma_\perp + f_\perp}{m_-} - \omega^2\right) - \frac{(\gamma'_\perp - f_\perp)^2}{m_+ m_-} = \frac{(\omega^2 - \omega_\perp^2)(\omega^2 - \Omega_+^2)\,(\omega^2 - \Omega_-^2)}{\omega^2 - c^2k^2} = 0, \tag{2.15}$$

gives one acoustic ($\omega_\perp^2$) and two polariton ($\Omega_\pm^2$) branches.

Neglecting the field effects and solving Eqs.(2.13-15) in the long-wavelength limit we obtain the dispersion laws of the acoustic ($\omega_\sigma^2$) and optical ($\Omega_\sigma^2$) phonons:

$$\omega_\sigma^2(k) = 2\frac{\gamma_\sigma(k) + \gamma'_\sigma(k)}{M} \approx v_\sigma'^{\,2}\, k^2, \tag{2.16}$$

$$\Omega_\sigma^2(k) = \frac{\gamma_\sigma(k)}{\mu} - 2\frac{\gamma_\sigma(k) + \gamma'_\sigma(k)}{M} \approx \Omega_0^2 - v_\sigma^2\, k^2. \tag{2.16'}$$

It allows us to express $\gamma_\sigma(k)$ and $\gamma'_\sigma(k)$ in terms of the conventional parameters:

$$\gamma_\sigma(k) \approx \mu\Omega_0^2 + \mu\, k^2\left(v_\sigma'^{\,2} - v_\sigma^2\right), \tag{2.17}$$

$$\gamma'_\sigma(k) \approx -\mu\Omega_0^2 + \mu\, k^2\left[v_\sigma^2 + v_\sigma'^{\,2}\left(\frac{M}{2\mu} - 1\right)\right], \tag{2.17'}$$

where $M$ is the total mass of the elementary cell, $v'_\sigma$ and $v_\sigma$ are the velocities of the acoustic and optical phonons with a given polarization, and $\Omega_0^2 = \gamma\,/\,\mu$ is the optical activation frequency.

The physical effects of the photon-phonon interaction become substantial near the cross-resonance point which is located in the long-wavelength region. In this case one can show that the acoustic branches remain unaffected by the field; whereas the interaction of the optical modes with the field leads to the uniform up-shift of the longitudinal branch, $\omega^2 = \Omega_\parallel^2(k) + d^2$, and splits the transverse phonons into two polariton branches defined by the well-known equation [18]:

$$\left(\omega^2 - \Omega_+^2\right)\left(\omega^2 - \Omega_-^2\right) = \left(\omega^2 - c^2k^2\right)\left(\omega^2 - \Omega_\perp^2\right) - d^2\omega^2 = 0. \tag{2.18}$$

The features of this approximation were analyzed in Chapter 1.1. We only mention that the lower polariton branch $\Omega_-^2(k)$ extends over both acoustic bands and reaches its maximum, $\Omega_{\max}^2$, at the point $k_{\max} \approx (2d\Omega_{\max}/v_\perp c)^{1/2}$, near the center of the Brillouin zone. The longitudinal branch, $\Omega_\parallel^2(k) + d^2$, overlaps the top part of the polariton gap and reaches its minimum, $\Omega_{\min}^2$, at the boundary of the Brillouin zone. The spectral gap, with no modes of any kind inside, is located between $\Omega_{\max}^2$ and $\Omega_{\min}^2$ [Fig. 1].

## 2.2. Polariton local states near the bottom of the gap

If a host ion at the site $\mathbf{r} = 0$ of the positive sublattice is replaced with an impurity ion of the same charge, it causes local deviations of the crystal density and the elastic constants. To account for these facts we need to add extra terms to the right hand side of Eq.(2.1). For the positive and negative sublattices, respectively, these terms are:

$$\delta \mathbf{f}^- (\mathbf{r}) = \left\{ \omega^2 \delta m_- \mathbf{U}_- (0) - \frac{\delta\nu}{n^2} \sum_{\mathbf{n}} \mathbf{n} \left[ \mathbf{n}\mathbf{U}_- (0) - \mathbf{n}\mathbf{U}_- (\mathbf{n}) \right] \right\} \delta_{\mathbf{r}\,0} \tag{2.19}$$

and

$$\delta \mathbf{f}^- (\mathbf{r}) = -\frac{\delta\nu}{n^2} \sum_{\mathbf{n}} \mathbf{n} \left[ \mathbf{n}\mathbf{U}_+ (0) - \mathbf{n}\mathbf{U}_- (\mathbf{n}) \right] \delta_{\mathbf{r}\,\mathbf{n}}, \tag{2.19'}$$

where vectors $\mathbf{n}$ denote radius-vectors of the impurity nearest neighbors, $\nu$ and $\delta\nu$ are the elastic constant of the near-neighbor bonds and its impurity-induced variation, and $\delta m_-$ is the difference between the masses of an impurity and a host ion.

The dynamical equation (2.5) is now modified:

$$\begin{pmatrix} \hat{\mathbf{D}} + \hat{\mathbf{F}} - \omega^2 m_+ & \hat{\mathbf{D}}' - \hat{\mathbf{F}} \\ \hat{\mathbf{D}}' - \hat{\mathbf{F}} & \hat{\mathbf{D}} + \hat{\mathbf{F}} - \omega^2 m_- \end{pmatrix} \begin{pmatrix} \mathbf{A}_+ \\ \mathbf{A}_- \end{pmatrix} = \frac{1}{N} \begin{pmatrix} \mathbf{B}_+ \\ \mathbf{B}_- \end{pmatrix} \tag{2.20}$$

where $N$ is the number of ions in one sublattice, and

$$\mathbf{B}_{+} = \omega^2 \delta m_{+} \mathbf{U}_{+} - \frac{\delta\nu}{n^2} \sum_{\mathbf{n}} \mathbf{n}(\mathbf{n}\mathbf{U}_{+} - \mathbf{U}_{\mathbf{n}}) \ , \tag{2.21}$$

$$\mathbf{B}_{-} = \frac{\delta\nu}{n^2} \sum_{\mathbf{n}} \mathbf{n} \left[\mathbf{n}\mathbf{U}_{-} - \mathbf{U}_{\mathbf{n}} \exp\left(-i\mathbf{k}\mathbf{n}\right)\right] \ . \tag{2.21'}$$

Here we denote $\mathbf{U}_{-} = \mathbf{U}_{-}(0)$, and all $\mathbf{U}_{-}(\mathbf{n})$ appear only in the combinations $\mathbf{U}_{\mathbf{n}} = \mathbf{n}\mathbf{U}_{-}(\mathbf{n})$ because the ion-ion forces are central.

Let us denote the matrix in Eq.(2.20) as $\hat{\mathbf{L}}$. It has the matrix elements $\mathbf{L}^{\alpha\alpha'}_{\varepsilon\varepsilon'}$ and acts on the Cartesian ($\alpha = 1, 2, 3$) and the sublattice ($\varepsilon = \pm$) indexes of the amplitudes $\mathsf{A}^{\alpha}_{\varepsilon}$. In the isotropic approximation this matrix can be decomposed,

$$\hat{\mathbf{L}} = \mathbf{L}_{\parallel} \otimes \hat{\mathbf{P}}_{\parallel} + \mathbf{L}_{\perp} \otimes \hat{\mathbf{P}}_{\perp} \, , \tag{2.22}$$

where $2 \times 2$-matrices $\mathbf{L}_{\sigma}$, operating on the sublattice indexes, are defined as follows:

$$\mathbf{L}_{\sigma} = \begin{pmatrix} l^{-}_{\sigma} & l'_{\sigma} \\ l'_{\sigma} & l^{-}_{\sigma} \end{pmatrix} = \begin{pmatrix} \gamma_{\sigma} + f_{\sigma} - \omega^2 m_{-} & \gamma'_{\sigma} - f_{\sigma} \\ \gamma'_{\sigma} - f_{\sigma} & \gamma_{\sigma} + f_{\sigma} - \omega^2 m_{-} \end{pmatrix} . \tag{2.23}$$

The inverse matrix,

$$\hat{\mathbf{G}} = \mathbf{L}^{-1}_{\parallel} \otimes \hat{\mathbf{P}}_{\parallel} + \mathbf{L}^{-1}_{\perp} \otimes \hat{\mathbf{P}}_{\perp} = \mathbf{G}_{\parallel} \otimes \hat{\mathbf{P}}_{\parallel} + \mathbf{G}_{\perp} \otimes \hat{\mathbf{P}}_{\perp} , \tag{2.24}$$

where $\mathbf{G}_{\sigma}$ have the following elements:

$$\begin{pmatrix} g^{-}_{\sigma} & g'_{\sigma} \\ g'_{\sigma} & g^{-}_{\sigma} \end{pmatrix} = \frac{1}{\left(\gamma_{\sigma} + f_{\sigma} - \omega^2 m_{+}\right)\left(\gamma_{\sigma} + f_{\sigma} - \omega^2 m_{-}\right) - \left(\gamma'_{\sigma} - f_{\sigma}\right)^2} \begin{pmatrix} l^{-}_{\sigma} & -l'_{\sigma} \\ -l'_{\sigma} & l^{-}_{\sigma} \end{pmatrix} , \tag{2.25}$$

is the Green's function of the system in the momentum representation. The poles of its matrix elements,

$$g_{\parallel}(\omega, \mathbf{k}) \ \propto \ \left(\omega^2 - \omega^2_{\parallel}\right)^{-1} \left(\omega^2 - \Omega^2_{\parallel} - d^2\right)^{-1} , \tag{2.26}$$

$$g_{\perp}(\omega, \mathbf{k}) \ \propto \ \left(\omega^2 - \omega^2_{\perp}\right)^{-1} \left(\omega^2 - \Omega^2_{-}\right)^{-1} \left(\omega^2 - \Omega^2_{-}\right)^{-1} . \tag{2.26'}$$

define the dispersion laws of the normal modes of the pure crystal.

Solving Eq.(2.20) with the help of Eqs.(2.23-2.25), one can obtain Fourier amplitudes of the ion displacements, $\mathbf{A}_{-}(\mathbf{k})$ and $\mathbf{A}_{-}(\mathbf{k})$, and the displacements themselves:

$$\mathbf{U}_{-}(\mathbf{r}) = \sum_{\sigma} \int_{(\mathbf{k})} \mathbf{e}_{\sigma}(\mathbf{k}) \otimes \mathbf{e}_{\sigma}(\mathbf{k}) \left(g_{\sigma}^{-}\mathbf{B}_{-} + g_{\sigma}^{\prime}\mathbf{B}_{-}\right) \exp\left(i\mathbf{kr}\right), \qquad (2.27)$$

$$\mathbf{U}_{-}(\mathbf{r}) = \sum_{\sigma} \int_{(\mathbf{k})} \mathbf{e}_{\sigma}(\mathbf{k}) \otimes \mathbf{e}_{\sigma}(\mathbf{k}) \left(g_{\sigma}^{\prime}\mathbf{B}_{-} + g_{\sigma}^{-}\mathbf{B}_{-}\right) \exp\left(i\mathbf{kr}\right), \qquad (2.27')$$

where the symbol $\int_{(\mathbf{k})}$ denotes $(1/N)\sum_{\mathbf{k}} \approx (a/2\pi)^3 \int d\mathbf{k}$, with the wave vectors taken from the first Brillouin zone only.

Substitution of $\mathbf{B}_{+}$ and $\mathbf{B}_{-}$, given by Eqs.(2.21-2.21'), into Eqs.(2.27-2.27') allows one to express all displacements in terms of $\mathbf{U}_{-}$ and $U_{\mathbf{n}}$, and then obtain a closed system of equations for these variables. In the case of the *isotope impurity*, we set $\delta\nu = 0$ and this system of *the spectral equations* reads:

$$\mathbf{U}_{-} = \omega^2 \delta m_{-} \sum_{\sigma} \int_{(\mathbf{k})} g_{\sigma}^{-} \, \mathbf{e}_{\sigma}(\mathbf{k}) \otimes \mathbf{e}_{\sigma}(\mathbf{k}) \, \mathbf{U}_{-}. \qquad (2.28)$$

This equation can be simplified with the help of the crystal symmetry. It is known that under any point transformation $\hat{\mathbf{Q}}$ the polarization vectors of the normal modes transform as follows: $\mathbf{e}(\hat{\mathbf{Q}}\mathbf{k}) = \hat{\mathbf{Q}}^{-1}\mathbf{e}(\mathbf{k})$. Taking into account that the eigen frequencies remain invariant, $\omega^2(\hat{\mathbf{Q}}\mathbf{k}) = \omega^2(\mathbf{k})$, and the Brillouin zone maps exactly into itself, one can show that the integrals in Eq.(2.28) present the group-invariant tensors:

$$\int_{(\hat{\mathbf{Q}}\mathbf{k})} g_{\sigma}(k) \, \mathbf{e}_{\sigma}\left(\hat{\mathbf{Q}}\mathbf{k}\right) \otimes \mathbf{e}_{\sigma}\left(\hat{\mathbf{Q}}\mathbf{k}\right) = \hat{\mathbf{Q}}^{-1} \left[\int_{(\mathbf{k})} g_{\sigma}(k) \, \mathbf{e}_{\sigma}(\mathbf{k}) \otimes \mathbf{e}_{\sigma}(\mathbf{k})\right] \hat{\mathbf{Q}}. \qquad (2.29)$$

In the cubic system any group-invariant operator must be proportional to the identity operator, because the point group includes non-collinear axis of different order.

Therefore, vector $\mathbf{U}_-$ in Eq.(2.28) can be chosen arbitrary, whereas the frequencies of the excitations are defined by the equation:

$$1 = \frac{\omega^2 \delta m_-}{3} \int_{(\mathbf{k})} \left( g_{\|}^- + 2 g_{\perp}^- \right) = \omega^2 \delta m_- I^- \left( \omega^2 \right), \tag{2.30}$$

which generalizes Eq.(1.5).

All solutions of Eqs.(2.28, 2.30) can be divided into two classes: the extended and local states. Since the impurity destroys the translational symmetry of the crystal, any state now presents a superposition of all normal modes available in the first Brillouin zone. For the extended states, corresponding to the scattering states with the well-defined wave vectors, frequencies fall into the bands of a pure crystal. The local states, dependent upon the value of the parameter $\delta m_-$ in Eq.(2.30), may arise inside the bandsgaps. From the structure of $g_\sigma(\omega, \mathbf{k})$ it might seem that when the frequency is close to a particular band, the modes from it dominate in the corresponding state. However, because contributions to $I^- \left( \omega^2 \right)$ from the near and distant bands depends on their densities of states, direct calculations are required here.

As we mentioned, the function $\Omega_-^2(k)$ reaches its maximum value $\Omega_{\max}^2$ at $k = k_{\max}$, and its expansion around $k_{\max}$ , given by Eq.(1.11), starts with the quadratic term. It immediately shows that the integral in the left-hand side of Eq.(2.30) diverges at $\omega = \Omega_{\max}$ due to the contribution from the lower polaritons branch. Therefore, considering $\omega$ close to the bottom of the spectral gap, we can omit $g_{\|}^-$ from Eq.(2.30) and rewrite $\int_{(\mathbf{k})} g_{\perp}^-$ using the density of states in the lower polaritons band $\rho_-(\varepsilon)$:

$$I_{\perp}^-(\omega^2) = \frac{2}{3} \left( \frac{a}{2\pi} \right)^3 \int g_{\perp}^- d\mathbf{k} = \frac{2}{3} \int_C \frac{\mathsf{F}(k) \rho_-(\varepsilon) d\varepsilon}{\omega^2 - \varepsilon}, \tag{2.31}$$

where $\mathsf{F}(k)$ denotes all factors of $g_\perp^-$, other than $\left[\omega^2-\Omega_-^2(k)\right]^{-1}$.

$$\mathsf{F}(k)=\frac{\left(\omega^2-c^2k^2\right)\left[\gamma_\perp(k)+f_\perp(k)-m_-\omega^2\right]}{m_-m_-\left[\omega^2-\Omega_-^2(k)\right]\left[\omega^2-\omega_\perp^2(k)\right]}. \tag{2.32}$$

The function $\rho_-(\varepsilon)$ in Eq.(2.31) is defined on the complex $\varepsilon$-plane, cut from 0 to $\Omega_{\max}^2$. The contour $C$ runs from 0 to $\Omega_{\max}^2$ along the upper side of the cut (it corresponds to the integration over $k<k_{\max}$), turns around its right edge and returns along the lower side of the cut to the point $\Omega_0^2-\Delta_\perp$ fixed by the bottom of the phonon band. The density of states has the usual Kohn's form, $\rho_-(\varepsilon)\propto\varepsilon^{1/2}$, at the bottom of the polariton band, and the "square-root"- singularity at its top, $\rho_-(\varepsilon)\propto\left(\Omega_{\max}^2-\varepsilon\right)^{-1/2}$. In the case $\omega^2-\Omega_{\max}^2\ll\Omega_{\max}^2$, the leading contribution to $I_\perp^-(\omega^2)$ comes from the vicinity of $\Omega_{\max}^2$. Therefore, considering $\omega^2$ from this region, we can replace the exact density of states in Eq.(2.31) with its asymptote given by Eq.(1.19). Taking into account that $k-k_{\max}=\mp\left(\Omega_{\max}^2-\varepsilon\right)^{1/2}/2v_\perp$ at the upper and lower sides of the cut, and expanding $\mathsf{F}(k)$ around $k_{\max}$ in Eq.(2.31), we obtain:

$$I_\perp^-(\omega^2)\propto\int_0^{\Omega_{\max}^2}\frac{\left[\mathsf{F}_0-z^{1/2}\mathsf{F}_0'/2v_\perp+\cdots\right]dz}{z^{1/2}\left[\Delta(\omega)+z\right]}+\int_0^{\Delta_\perp-\Delta_1}\frac{\left[\mathsf{F}_0+z^{1/2}\mathsf{F}_0'/2v_\perp+\cdots\right]dz}{z^{1/2}\left[\Delta(\omega)+z\right]}. \tag{2.33}$$

where we denote $\Delta(\omega)=\omega^2-\Omega_{\max}^2$, and $z=\Omega_{\max}^2-\varepsilon$.

Rescaling the integration variable, $z\to z\,\Delta(\omega)$, one can show that the contributions to $I_\perp^-(\omega^2)$ from all terms of expansion of $\mathsf{F}(k)$ tend to zero in the limit $\omega\to\Omega_{\max}$, except for the first two terms. Further elementary integration gives the singular part of the considered integral:

$$I_\perp^-(\omega^2)\approx\frac{a(ak_{\max})^2}{3\pi v_\perp\sqrt{\omega^2-\Omega_{\max}^2}}\times\left.\frac{\left(\omega^2-c^2k^2\right)\left[\gamma_\perp(k)+f_\perp(k)-m_-\omega^2\right]}{m_-m_-\left[\omega^2-\Omega_-^2(k)\right]\left[\omega^2-\omega_\perp^2(k)\right]}\right|_{k_{\max}}. \tag{2.34}$$

This result is asymptotically exact since all omitted terms are regular at $\omega\to\Omega_{\max}$.

Recalling that $ak_{\max} \ll 1$, $v_\perp k_{\max} \ll \Omega_0$, $ck_{\max} \gg \Omega_0$ and $\omega \approx \Omega_{\max} \approx \Omega_0$; and using Eqs.(2.16-17′) and Eq.(1.11′), we can simplify the second factor of Eq.(2.34) and transform the spectral equation (2.30) into the form:

$$\sqrt{\omega^2 - \Omega_{\max}^2} \approx -\frac{a\,(ak_{\max})^2}{3\,\pi\,v_\perp} \times \frac{\Omega_0^2\, m_- \delta m_-}{M\, m_-} = -\frac{a\,(ak_{\max})^2}{3\pi v_\perp} \times \frac{\Omega_0^2\,\delta\mu}{\mu} \qquad (2.35)$$

This result resembles Eq.(1.12) and demonstrates the absence of the lower threshold for the isotope-induced local states.

In a general case of a *non-isotope* impurity the spectral system contains 11 variables, namely, three components of the impurity displacement $\mathbf{U}_- = \mathbf{U}_-(0)$, and the radial projections of its eight nearest neighbors $\mathsf{U}_\mathbf{n} = \mathbf{n}\mathbf{U}_-(\mathbf{n})$. The system can be further simplified with the help of the crystal symmetry. The exact point group of a cubic crystal includes the space inversion. Therefore, all excitations can be classified by their spatial parity.

For *odd states*, when $\mathbf{U}_\pm(-\mathbf{r}) = -\mathbf{U}_\pm(\mathbf{r})$, one can see that $\mathbf{U}_-$ and $\mathbf{B}_-$ are equal to zero and the rank of the spectral system reduces from 11 to 4. Considering the displacements of four negative ions at one face of the elementary cell as independent variables [Fig.2] we obtain from Eqs.(2.24, 2.24′) the following system:

$$\sum_{s'=1}^{4} \mathsf{M}_{ss'}\mathsf{U}_{s'} = -\frac{n^2}{2\delta\nu}\,\mathsf{U}_s\,, \qquad (2.36)$$

where index $s$ enumerates the chosen ions, vectors $\mathbf{n}_s$ denote their radius-vectors, $\mathsf{U}_s = \mathbf{n}_s\mathbf{U}_-(\mathbf{n}_s)$, and the matrix $\mathsf{M}_{ss'}$ is defined by the equation:

$$\mathsf{M}_{ss'} = M(\mathbf{n}_s,\, \mathbf{n}_{s'}) = \sum_\sigma \int_{(\mathsf{k})} g_\sigma^-(\mathbf{e}_\sigma\mathbf{n}_s)(\mathbf{e}_\sigma\mathbf{n}_{s'})\sin(\mathbf{k}\mathbf{n}_s)\sin(\mathbf{k}\mathbf{n}_{s'}). \qquad (2.37)$$

Using transformation properties of the integrand in Eq.(2.37) one can show that this matrix is the invariant of the point-group transformations, $M(\hat{\mathbf{Q}}\mathbf{n},\, \hat{\mathbf{Q}}\mathbf{n}') = M(\mathbf{n},\, \mathbf{n}')$.

Therefore, the elements of the symmetric matrix $M_{ss'}$ are equal for equivalent pairs of ions:

$$\begin{aligned} M_{11} &= M_{22} = M_{33} = M_{44}, \\ M_{12} &= M_{23} = M_{34}, \\ M_{13} &= M_{24}. \end{aligned} \tag{2.38}$$

In this case Eq.(2.36) can be rewritten in the form:

$$\begin{pmatrix} M_{11} - M_{13} - \lambda & 0 & 0 & 0 \\ 0 & M_{11} - M_{13} - \lambda & 0 & 0 \\ M_{13} & M_{12} & M_{11} + M_{13} - \lambda & 2M_{12} \\ M_{12} & M_{13} & 2M_{12} & M_{11} + M_{13} - \lambda \end{pmatrix} \begin{pmatrix} U_1 \\ U_2 \\ U_3 - U_1 \\ U_4 - U_2 \end{pmatrix} = 0. \tag{2.39}$$

which gives us three spectral equations defining the frequencies of the odd states:

$$-\frac{n^2}{2\delta\nu} = \lambda_{\pm} = M_{11} + M_{13} \pm 2M_{12}, \tag{2.40}$$

$$-\frac{n^2}{2\delta\nu} = \lambda_0 = M_{11} - M_{13}. \tag{2.40'}$$

For $\lambda_{\pm}$-states Eqs.(2.39-2.40) give $U_1 = U_2 = 0$ and $U_3 = \pm U_4$. Recalling that we consider the antisymmetric states, one can see that, in the $\lambda_-$-state, the elementary cell inclosing a defect experiences "rhombic" deformations. In the $\lambda_-$-state, the ion displacements are anti-phased, what leads to "tetragonal" deformations. In the $\lambda_0$-state, $U_3 = U_1/2$ and $U_4 = U_2/2$, whereas $U_1$ and $U_2$ are independent. This corresponds to the combined "tetra-rhombic" deformations of the elementary cell.

Considering the states near the bottom of the gap we can evaluate the matrix elements $M_{ss'}$ and find the eigen frequencies. In the limit $\omega \to \Omega_{\max}$, factor

$\left[\omega^2 - \Omega_-^2(k)\right]^{-1}$of $g_\perp^-(\omega, k)$ causes a divergence of the integrals in Eq.(2.37). Therefore, similar to the isotope impurity case, the long-wavelength regions ($k \sim k_{\max}$) of the transverse integrals give the major contributions to $\mathsf{M}_{ss'}$ for $\omega^2 - \Omega_{\max}^2 \ll \Omega_{\max}^2$. Retaining in Eq.(2.37) only the first terms of the expansions of sin-functions, and using the identities:

$$\int_{(\mathbf{k})} f(k) k^\alpha k^\beta k^\sigma k^\beta = \frac{1}{15}\left(\delta^{\alpha\beta}\delta^{\sigma\beta} + \delta^{\alpha\sigma}\delta^{\beta\beta} + \delta^{\alpha\beta}\delta^{\beta\sigma}\right)\int_{(\mathbf{k})} f(k) k^4. \quad (2.41)$$

$$\int_{(\mathbf{k})} f(k) k^\alpha k^\beta = \frac{1}{3}\delta^{\alpha\beta}\int_{(\mathbf{k})} f(k) k^2. \quad (2.41')$$

where $f(k)$ is an arbitrary invariant function, we obtain:

$$\mathsf{M}_{ss'} \approx \frac{1}{3}\left\{(\mathbf{n}_s\mathbf{n}_{s'})^2 - \frac{n^4 + 2(\mathbf{n}_s\mathbf{n}_{s'})^2}{5}\right\}\int_{(\mathbf{k})} k^2 g_\perp^-. \quad (2.42)$$

Substitution of this result back into Eqs.(2.40-40′) leads us to the following results:

$$\lambda_0 \approx \frac{1}{5}\left[n^4 - (\mathbf{n}_1\mathbf{n}_3)^2\right]\int_{(\mathbf{k})} k^2 g_\perp^-. \quad (2.43)$$

$$\lambda_\pm \approx \frac{1}{5}\left\{(\mathbf{n}_1\mathbf{n}_3)^2 + \frac{n^4}{3} \pm 2\left[(\mathbf{n}_1\mathbf{n}_2)^2 - \frac{n^4}{3}\right]\right\}\int_{(\mathbf{k})} k^2 g_\perp^-. \quad (2.43')$$

Taking into account $(\mathbf{n}_1\mathbf{n}_2) = -(\mathbf{n}_1\mathbf{n}_3) = a^2/4$ and $n^2 = 3a^2/4$, and evaluating the integral in these equations in the way similar to Eqs.(2.30-2.34), we obtain:

$$\lambda_0 = \lambda_- = \frac{a^4}{10}\int_{(\mathbf{k})} k^2 g_\perp^- \approx -\frac{a^3\,(ak_{\max})^4}{20\,\pi\,v_\perp\sqrt{\omega^2 - \Omega_{\max}^2}} \times \frac{m_-}{M m_-} \quad (2.44)$$

This provides the unique spectral equation for all "tetragonal" modes:

$$\sqrt{\omega^2 - \Omega_{\max}^2} \approx \frac{\delta\nu}{\gamma} \times \Omega_0^2\left(\frac{m_-}{M}\right)^2 \times \frac{2\,a\,(ak_{\max})^4}{15\,\pi\,v_\perp}. \quad (2.45)$$

This result shows that the odd local states arise upon an infinitesimally small strengthening of the elastic bonds around the impurity. Similar to the isotope impurity case, this effect is due to the singularity of the density of states in the lower polariton band.

Eq.(2.45), compared to Eq.(2.35), has an additional small factor, $(ak_{\max})^2$. Therefore, for the same relative deviations, $\delta\nu/\nu$ and $\delta\mu/\mu$, the odd local states lie much closer to the bottom of the gap than the states associated with the isotope impurity. Moreover, these states are less sensitive to variations of the impurity parameters than the isotope-induced local states. This fact reveals itself in an extreme form for "rhombic" modes corresponding to $\lambda_-$. From Eq.(2.43′) follows $\lambda_- = 0$, what means that, within the approximations used, the $\lambda_-$-states appear right at the bottom of the gap for any value of $\delta\nu$. Accounting for the higher-order terms in expansions of the sin-functions in Eq.(2.37) will separate these modes from the bottom of the gap but the separation, $\sqrt{\omega^2 - \Omega^2_{\max}} \propto \delta\nu\ (ak_{\max})^6$, will remain the smallest among the considered local states.

For *even states*, when $\mathbf{U}_\pm(-\mathbf{r}) = \mathbf{U}_\pm(\mathbf{r})$, the spectral system contains 7 independent variables. Those are components of the impurity displacement, $\mathbf{U}_-$, and the radial projections of the displacements of four chosen neighboring ions, $U_s = \mathbf{n}_s\mathbf{U}_-(\mathbf{n}_s)$. The matrix in the corresponding spectral system involves the integrals of the Green's function elements similar to Eq.(2.37). Considering states near the bottom of the gap, we again can retain in these integrals only the transverse terms and use the power expansions of non-singular factors of the integrands. Due to the dominant contribution into these integrals from the small-$k$ regions, we have $\int_{(\mathbf{k})} (ak)^2 g^{\pm}_{\perp} \ll \int_{(\mathbf{k})} g^{\pm}_{\perp}$. Therefore, since the local states near the bottom of the gap are "made" of the long-wavelength polaritons, we can disregard the exponential factors in the matrix elements of the spectral system [$\exp(\pm i\mathbf{kn}) \approx 1$] and neglect in Eqs.(2.21-2.21′) the differences between the displacements of identical ions within the elementary cell [$\mathbf{U}_-(\mathbf{n}) = \mathbf{U}_-$ =const]. These approximations lead to the following spectral system

for even states:

$$\begin{pmatrix} \mathbf{U}_- \\ \mathbf{U}_- \end{pmatrix} \approx \begin{pmatrix} I_\perp^- & I_\perp' \\ I_\perp' & I_\perp^- \end{pmatrix} \begin{pmatrix} \omega^2\delta m_- - 8\delta\nu/3 & 8\delta\nu/3 \\ 8\delta\nu/3 & -8\delta\nu/3 \end{pmatrix} \begin{pmatrix} \mathbf{U}_- \\ \mathbf{U}_- \end{pmatrix}. \tag{2.46}$$

The corresponding spectral equation reads:

$$\frac{8\delta\nu}{3}\left(I_\perp^- + I_\perp^- - 2I_\perp'\right) - \omega^2\delta m_- I_\perp^- + 1 = \frac{8\omega^2\delta\nu\delta m_-}{3}\left(I_\perp^- I_\perp^- - I_\perp'^2\right). \tag{2.47}$$

where all $I$-factors are straightforward to evaluate near the bottom of the gap:

$$I_\perp^\pm(\omega^2) = \frac{2}{3}\int_{(\mathbf{k})} g_\perp^\pm \approx \frac{a\left(ak_{\max}\right)^2}{3\pi v_\perp\sqrt{\omega^2-\Omega_{\max}^2}} \times \frac{\mu - m_\mp}{m_- m_-}. \tag{2.48}$$

$$I_\perp'(\omega^2) = \frac{2}{3}\int_{(\mathbf{k})} g_\perp' \approx \frac{a\left(ak_{\max}\right)^2}{3\pi v_\perp\sqrt{\omega^2-\Omega_{\max}^2}} \times \frac{\mu}{m_- m_-}. \tag{2.48'}$$

The right-hand side of Eq.(2.47) is proportional to the determinant of the degenerate operator, the transverse propagator, and it must be equal to zero identically. Substitution of Eqs.(2.48-2.48′) into Eq.(2.47) shows this explicitly and leads to the final spectral equation for even states:

$$\sqrt{\omega^2-\Omega_{\max}^2} = \left[\frac{8\delta\nu}{3\mu} - \Omega_0^2\frac{\delta\mu}{\mu}\right] \times \frac{a\left(ak_{\max}\right)^2}{3\pi v_\perp}. \tag{2.49}$$

The ion displacements in these states satisfy the relationship of the optical type:

$$m_-^2\mathbf{U}_- + m_-^2\mathbf{U}_- = 0. \tag{2.50}$$

If we set $\delta\nu = 0$ in Eq.(2.49) it reproduces Eq.(2.35) obtained earlier for the isotope impurity, which has a solution only for $\delta\mu < 0$. In a general case the even local states exist only if variations of the impurity parameters satisfy the inequality:

$$\delta\nu > \frac{3}{8}\Omega_0^2\delta\mu\ . \tag{2.51}$$

### 2.3. Anisotropy-induced threshold for the local states.

All local states considered in this and the previous chapters arise in the polariton gap upon infinitesimally small variations of the impurity parameters. This is in contrast with 3-D phonon systems where a lower threshold for the impurity strength always exists. The general theorem regarding the existence of the threshold for local states in bandgaps of the periodic systems was formulated in Ref.[23]. However, the proof suggested the finite values of density of states in the entire band of pure system. In our models the absence of the threshold is provided by the singularity of the density of states in the lower polariton band, $\rho_{-}\left(\omega^{2}\right) \propto \left(\Omega_{\max}^{2}-\omega^{2}\right)^{-1/2}$. This singularity is associated with the long-wavelength polaritons and is caused by the isotropy and negative dispersion of the parent phonon branch. However, even a weak crystal anisotropy can eliminate the singularity of the polariton density of states.

In the cubic crystals, the anisotropic terms of the phonon dispersion law appear beyond the quadratic approximation:

$$\Omega_{\perp}^{2}(\mathbf{k})=\Omega_{0}^{2}-v_{\perp}^{2}k^{2}+\chi\,\Omega_{0}^{2}\,(ak)^{4}\,F\left(\hat{\mathbf{k}}\right), \tag{2.52}$$

where $\chi$ is the small parameter, and $F\left(\hat{\mathbf{k}}\right)$ is some anisotropic function. Due to the anisotropic term, as one can see from Eq.(1.7), the position, $k_{\max}$, and the value of the maxima in the lower polariton branch, $\Omega_{\max}^{2}$, depend on the crystallographic direction. In the case of a weak anisotropy the first effect can be neglected, what leads to the following approximation of $\Omega_{-}^{2}(\mathbf{k})$ near the surface $\mathbf{k}^{2}=k_{\max}^{2}$ :

$$\Omega_{-}^{2}(\mathbf{k}) \approx \Omega_{\max}^{2}\left[1+\chi\ (ak_{\max})^{4}\ F\left(\hat{\mathbf{k}}\right)\right]-4v^{2}\left(k-k_{\max}\right)^{2}. \tag{2.53}$$

The small magnitude of the anisotropic term,

$$\left|\chi\,F\left(\hat{\mathbf{k}}\right)(ak_{\max})^{4}\right| \sim \chi\,\beta^{2}\,\Omega_{\max}^{2} \ll \Omega_{\max}^{2}, \tag{2.54}$$

allows us to evaluate the asymptote of the density of states:

$$\rho\left(\omega^2\right) \propto \oint_{\Omega_-(\mathbf{k})=\omega} d\sigma \left|\nabla_{\mathbf{k}}\Omega_-^2\left(\mathbf{k}\right)\right|^{-1} \propto \left(\Omega_{\max}^2 - \omega^2 + A\right)^{-1/2}. \tag{2.55}$$

Since the crystal anisotropy destroys the continuous degeneration of the polariton spectrum, it removes the singularity of the density of states from the bottom of the gap. The anisotropy-induced shift of the singularity,

$$A = \chi\ \left(ak_{\max}\right)^4\ \Omega_{\max}^2\ \left\langle\left|F\left(\hat{\mathbf{k}}\right)\right|\right\rangle\ . \tag{2.56}$$

where $\left\langle\left|F\left(\hat{\mathbf{k}}\right)\right|\right\rangle \sim 1$ is an "average" value of the anisotropic function, defines a finite threshold for the local polariton states:

$$\alpha_{\min} \sim A^{1/2}\ \beta^{-1}\Omega_0 \sim \chi^{1/2}\ \Omega_0^2. \tag{2.57}$$

# 3. A dipole-active atomic layer

The local polariton states considered in the previous chapters provide the "phonon assisted" localization of photons. However, the proximity of these states to the lower polariton band causes their high relaxation rate. Moreover, our estimates show that the field component of the local states is relativistically small. A suppression of the photon content of the polariton states and a small width of the crossover region are due to the fact that the typical momentum of the modes dominating in the local states, $k_{\max} \sim \beta^{1/2} a^{-1}$, greatly exceeds the cross-resonance momentum, $k_0 \sim \beta\, a^{-1}$. This, in turns, is the result of a strong disproportion between the phonon velocity and the speed of light.

The photon group velocity can be lowered in the medium placed in a waveguide. In this chapter we consider an atomically thin dielectric sheet (ionic 2D-crystal ) inside the parallel-plate waveguide. Due to a non-linear dispersion law of the waveguide modes, $\omega_n(k) = c\ \sqrt{(\pi n/2\,l)^2 + k^2}$, their group velocity is reduced in the long-wavelength region. The coherent interaction between the waveguide modes and the polarization waves produces new excitations - 2D-polaritons. Considering the waveguide width, $l$, as an adjustable parameter, we investigate the polariton local states and the localized waveguide modes.

## 3.1. Polaritons in the ionic 2D-crystal

Let us consider an atomically thin dielectric layer between two perfectly conducting sheets [Fig.4]. The layer presents a regular ionic 2D-crystal, which is stabilized in $z = 0$ plane by an external potential. A restraining potential increases the activation energy of the off-layer lattice vibrations and shifts the corresponding phonon modes

much higher than the modes with the in-plane polarization. A sub-micron crystal film grown on a substrate with the lattice parameter much smaller than that of the film can be a physical realization of this model. Assuming an infinitely strong confining potential we eliminate the off-plane phonons from our model. Among the remaining in-plane phonons, for the sake of simplicity, we consider only a single transverse dipole-active mode with the isotropic spectrum and negative dispersion. In the long-wavelength region we can use the standard approximation, $\Omega^2(k) \approx \Omega_0^2 - v^2k^2$. Since the activation frequency of this 2D-phonon mode is unaffected by the confining potential, we take for an estimate $\Omega_0 \sim v/a \sim 10^{11} \div 10^{13} Hz$.

The optical phonon excitations in a thin layer have a high relaxation rate, unless the induced electromagnetic radiation from its surface is compensated. In our model, it is provided by the coherent coupling between the lattice excitations and the eigen modes of the waveguide. In the parallel plate waveguide there are two types of propagating modes [Fig 4]. TM-modes (transverse-magnetic) involve electric field across the layer and, therefore, they cannot be activated in our model. Electric field in TE-modes (transverse-electric) is directed along the layer and they can be excited by the transverse-optical phonons. Introducing the surface polarization $Q(x,y)$ associated with these 2D-phonons and considering it together with the corresponding TE-modes of the waveguide, we obtain the following system of equations:

$$c^2 \frac{\partial^2 E_{\mathbf{k}}}{\partial z^2} + \left(\omega^2 - c^2k^2\right) E_{\mathbf{k}} = -4\pi\omega^2 Q_{\mathbf{k}} \delta(z), \tag{3.1}$$

$$\left[\omega^2 - \Omega^2(k)\right] Q_{\mathbf{k}} = -\frac{ad^2}{4\pi} E_{\mathbf{k}}(0), \tag{3.2}$$

where $Q_{\mathbf{k}}$ and $E_{\mathbf{k}}(z)$ are the Fourier amplitudes of the polarization and the electric fields, $\mathbf{k}$ is a 2D-wave vector, $d$ is the ion plasma frequency. For later convenience we

use below the dimensionless variables $lk \to k$, $l\omega/c \to \omega$, and $l\Omega/c \to \Omega$, so that $\Omega^2(k) \approx \Omega_0^2 - \beta^2 k^2$, and $\Omega_0 \sim k_0 \sim \eta\beta$, where $\eta = l/a$ is a large parameter.

The electric field in Eq.(3.1) is confined between the conducting plates and its normal derivative at the surface of the dielectric sheet has a discontinuity caused by the surface polarization. Solving Eqs.(3.1-3.2) under these conditions, we obtain the following dispersion equation:

$$\frac{\Omega^2 - \omega^2}{\omega^2} = \delta \, \frac{\tan\sqrt{\omega^2 - k^2}}{\sqrt{\omega^2 - k^2}} . \tag{3.3}$$

where $\delta = al\,d^2/2\,c^2 \sim \eta\beta^2$ is a small parameter.

This equation defines a series of 2D-polariton branches [Fig. 5.6] with their activation frequencies given by the equation:

$$\omega_n^2 - \Omega_0^2 = -\delta\,\omega_n \tan\omega_n . \tag{3.4}$$

Analysis of Eq.(3.4) shows that the upper ($n \geq 1$) branches have quadratic "large momenta" asymptotes,

$$\omega_n^2(k) \approx \omega_n^2 + k^2 \; ; \tag{3.5}$$

therefore, their frequency bands all overlap and form a common upper polariton band. The lower ($n = 0$) polariton branch is separated from the others by the polariton gap, bottom of which is set by the maximum of this branch.

Evaluation of the group velocity at the center of the Brillouin zone,

$$\left[\frac{d\omega_0^2(k)}{dk^2}\right]_{k=0} \propto -\beta^2 + \frac{\Omega_0^2 - \omega_0^2}{2\omega_0^2}\left(\frac{2\omega_0}{\sin 2\omega_0} - 1\right) \sim -\beta^2 + \frac{\delta\Omega_0^2}{3} , \tag{3.6}$$

shows that the lower branch has a negative dispersion if $l \lesssim \beta^{-2/3}a \sim 10^4 a$. In such narrow waveguides, the photon-phonon coupling is negligible and the phonon branch, with its maximum located at $k = 0$, remains practically unaffected by the field.

As $l$ increases, the polariton maximum moves away from $k = 0$, reaching the cross-resonance region, $k \sim k_0$, at $l \gtrsim \beta^{-2/3}a$. We restrict our further consideration to the case $l \gg \beta^{-2/3}a$, only. It guarantees that the maximum of the lower branch is located far away from $k_0$. In this region $k \gg \Omega, \omega$, and Eq.(3.3) can be approximated as follows:

$$\Omega^2 - \omega^2 \approx \frac{\delta}{2k^3}\omega^2 \left(\omega^2 + 2k^2\right) . \tag{3.7}$$

A positively defined solution of Eq.(3.7) gives the "large momenta" asymptote of the lower polariton branch:

$$\omega_0^2(k) \approx \Omega^2 \left(1 - \frac{\delta}{k}\right). \tag{3.8}$$

Its dispersion curve reaches the maximum at the point

$$k_{\max} \approx l \left(\frac{ad^2\Omega_0^2}{2v^2c^2}\right)^{1/3} \sim \eta\beta^{2/3} \gg 1. \tag{3.9}$$

where it sets the bottom of the polariton gap:

$$\Omega_{\max}^2 \approx \Omega_0^2 - 3\frac{l^2}{c^2}\left(\frac{avd^2\Omega_0^2}{2c^2}\right)^{2/3} \sim \Omega_0^2 - 3\beta^{4/3}\left(d^2\Omega_0\right)^{2/3}\frac{l^2}{c^2} . \tag{3.10}$$

In the immediate vicinity of $k_{\max}$, the polariton dispersion law can be presented as follows:

$$\omega_0^2(k) \approx \Omega_{\max}^2 - 3\beta^2\left(k - k_{\max}\right)^2 , \tag{3.11}$$

and the corresponding asymptote of the density of states has the form:

$$\rho(\omega^2) \propto \frac{k_{\max}}{2\pi\beta\sqrt{3\left(\Omega_{\max}^2 - \omega^2\right)}} \sim \frac{c}{a}\frac{\eta\beta^{2/3}}{\Omega_0\sqrt{\Omega_{\max}^2 - \omega^2}}. \tag{3.12}$$

Restoring the natural dimensionality of the variables and comparing our results with those obtained for 3D-polaritons,

$$k_{\max} \sim \beta^{1/2}a^{-1}, \quad \Omega_{\max}^2 \sim \Omega_0^2 - 2\beta d\Omega_0,$$

$$\rho(\omega^2) \propto \frac{\beta}{\Omega_0 \sqrt{\Omega_{\max}^2 - \omega^2}},$$

one can see that the maximum of the polariton curve in a thin layer is located closer to the cross-resonance point, $k_0 \sim \beta a^{-1}$, and the bottom of the gap is shifted toward the phonon activation frequency. Also, the singularity of the density of states is strengthened by the factor of $\beta^{-1/3} \sim 10^2$. Setting $\rho(\omega^2) \sim 1/\Delta$, where $\Delta$ is the width of the polariton band, one can estimate the frequency range where the singularity prevails:

$$\sqrt{\Omega_{\max}^2 - \omega^2} \sim \beta^{2/3} \frac{\Delta}{\Omega_0} \sim \beta^{2/3} \Omega_0 \,. \tag{3.13}$$

Comparing to the 3D-case, it is enlarged by the factor of $\beta^{-1/3}$, what broadens the region of the local states dominated by the long-wavelength modes.

### 3.2. The local states and localized waveguide modes

When a point-like defect is embedded in the dielectric layer, it modifies Eq.(3.2) as follows:

$$[\omega^2 - \Omega^2(k)\,]\, Q_{\mathbf{k}} = -\frac{ad^2}{4\pi} E_{\mathbf{k}}(0) + \frac{\alpha a^2 Q(0)}{4\pi S}, \tag{3.14}$$

where $Q(0)$ is the polarization of a defect and $S$ is the total area of the layer. The strength of the defect, $\alpha$, depends on its mobility and binding energy in a crystal. In the case of the isotope impurity, $\alpha = -\omega^2 \delta m/m$; for a non-isotope impurity or a structural defect we assume that $\alpha \sim \overline{\alpha}\,\Omega_0^2$, where $\overline{\alpha}$ is a numerical factor.

Solving Eqs.(3.1, 3.14) we obtain ( in the dimensionless variables $\omega, k$,and $\Omega$):

$$E_{\mathbf{k}}(z) = \frac{\alpha a^2 l\, Q(0)}{2\, S\, c^2} \times \frac{\omega^2 \sin\zeta \mathcal{Z}}{\zeta \cos\zeta} \times \left(\omega^2 - \Omega^2 + \delta \frac{\omega^2 \tan\zeta}{\zeta}\right)^{-1}, \tag{3.15}$$

where we denote $\mathcal{Z} = l^{-1}(l \pm z)$ and $\zeta = \sqrt{\omega^2 - k^2}$.

Using this equation one can express $Q_{\mathbf{k}}$ *via* the polarization of the defect, $Q(\mathbf{0})$, and obtain then the spectral equation for the local state:

$$1 = \frac{\alpha}{4\pi c^2}\left(\frac{a}{2\pi}\right)^2 \times \int d\mathbf{k}\left(\omega^2 - \Omega^2 + \delta\ \frac{\omega^2 \tan\zeta}{\zeta}\right)^{-1}. \tag{3.16}$$

When the frequency approaches $\Omega_{\max}$, the integral diverges at the "surface" $\mathbf{k}^2 = k_{\max}^2$. Near $\Omega_{\max}$ , using Eqs.(3.7, 3.11), we can approximate Eq.(3.16) as follows:

$$1 \approx \frac{\alpha}{2c^2}\left(\frac{a}{2\pi}\right)^2 \times \int_0^\infty \frac{kdk}{\omega^2 - \Omega_m^2 + 3\beta^2\ (k - k_m)^2}; \tag{3.17}$$

Retaining here only the singular part of the integral, we finally obtain:

$$\sqrt{\omega^2 - \Omega_m^2} \approx \frac{\alpha a\,(ak_m)}{8\pi\, c^2 \beta\sqrt{3}} \sim \overline{\alpha}\eta\beta^{5/3}. \tag{3.18}$$

Comparing to the 3D-case $\left(\sqrt{\omega^2 - \Omega_m^2} \sim \overline{\alpha}\eta\beta^2\right)$, the separation of the local state from the bottom of the gap is enlarged by the factor of $\beta^{-1/3}$.

Equation (3.18) gives the eigen frequency of the local state near the bottom of the gap. To find the localization radius of this state we calculate the spatial distribution of the electric and the polarization fields. The inverse Fourier transformation of Eq. (3.15) gives us:

$$E(z, \mathbf{r}) = \frac{\alpha\omega^2 a^2\ Q(0)}{4\pi\, l\, c^2} \times \int_{-\infty}^{\infty} \frac{dk\, k\ H_0(k\mathcal{R})\sin(\zeta\mathcal{Z})}{(\omega^2 - \Omega^2)\,\zeta\cos\zeta + \delta\omega^2\sin\zeta}\ , \tag{3.19}$$

where $H_0(k\mathcal{R})$ is the Hankel function of first kind, $\mathcal{R} = l^{-1}r$.

It follows from the spectral properties of the system that the denominator of the integrand, considered as a function of $\omega^2$, has a series of isolated simple zeroes:

$$F(\omega, k) = \left[\left(\omega^2 - \Omega^2\right)\zeta\cos\zeta + \delta\omega^2\sin\zeta\right] \propto \prod_n \left[\omega^2 - \omega_n^2(k)\right]\ , \tag{3.20}$$

where the index $n$ enumerates the polariton branches, $\omega_n^2(k)$. Since the frequency of the local state, $\omega$, lies in the polariton gap, all $k$-zeroes of $F(\omega, k)$ are removed from the $\mathrm{Re}\, k$-axis. Closing the integration contour in Eq.(3.19) through the upper half-plane, we can calculate the integral by the method of residuals:

$$E(z, \mathbf{r}) = \frac{i\alpha\omega^2 a^2 Q(0)}{2\,l\,c^2} \times \sum_{k_n} \mathrm{Res}\left\{H_0(k\mathcal{R}) \sin(\zeta\mathcal{Z}) \left[F(\omega, k)\right]^{-1}\right\}_{k_n^+} , \qquad (3.21)$$

where $k_n^-$ is the pole associated with $n$-th branch.

Near the bottom of the gap ($\omega \gtrsim \Omega_{\max}$) the factor of $F(\omega, k)$ presenting the lower polariton branch, $\omega^2 - \omega_0^2(k)$, is small for $k \sim k_{\max}$. It suggests that the poles of $[F(\omega, k)]^{-1}$ corresponding to the lower branch are located in the vicinity of $k_{\max}$. Using Eq.(3.11) one can find:

$$k_0^{\pm} = k_{\max} \pm i\sqrt{\frac{\omega^2 - \Omega_{\max}^2}{3\beta^2}} = k_{\max} \pm i\varkappa . \qquad (3.22)$$

For a weak defect $\varkappa \sim \overline{\alpha}\, k_{\max} \ll k_{\max}$ . as it follows from Eq.(3.18). Taking into account that $k_{\max} \sim \eta\beta^{2/3} \gg \Omega_{\max} \sim \eta\beta$, one can evaluate:

$$\mathrm{Res}\left[F(\omega, k)\right]_{k_0^+}^{-1} \approx \frac{\exp(-k_{\max})}{3\beta^2 \varkappa k_{\max}} . \qquad (3.23)$$

To find zeroes of $F(\omega, k)$ corresponding to the upper branches, we first impose the upper limitation on the width of the waveguide, so that $\beta^{-2/3}a \ll l \ll \beta^{-1}a$. In this case the phonon band lies well below the waveguide cut-off frequency and all high-order polariton branches are practically indistinguishable from the parent TE-modes. Recalling then Eq.(3.5), and taking into account that $\omega_n \approx \pi\left(n - \frac{1}{2}\right) \gg \Omega_0$, we obtain:

$$k_n^{\pm} = \pm\, i\sqrt{\omega_n^2 - \omega^2} \approx \pm\, i\omega_n , \qquad (3.24)$$

and the corresponding residuals:

$$\mathrm{Res}\left[F\left(\omega,k\right)\right]_{k_n^+}^{-1} \approx \frac{i\cos\omega_n}{\delta\,\omega^2}\,. \tag{3.25}$$

Finally, using Eqs.(3.21-25), we can find the large-distance asymptote of the electric field:

$$E(z,\mathbf{r}) \propto \mathcal{R}^{-1/2}\left[\frac{\exp\left(-\mathcal{R}\varkappa - z k_{\max}\right)}{6\,\beta^2\,\varkappa\,k_{\max}^{3/2}} + \sum_{n=1}^{\infty}\frac{\exp\left(-\mathcal{R}\omega_n\right)\sin\left(\omega_n\mathcal{Z}\right)\cos\omega_n}{\delta\omega^2\;\omega_n^{1/2}}\right]. \tag{3.26}$$

This result presents the field as the sum of contributions from all branches. However, because $\omega_n$ rapidly approaches $\pi\left(n-\frac{1}{2}\right)$ upon increase of the branch number, only several terms corresponding to the low-located branches can be retained in the sum. As it is seen from Eq.(3.26), the field is localized in radial directions, whereas its $z$-profile critically depends on the defect strength, $\overline{\alpha}$. For a weak defect, when $\varkappa \ll \omega_1$ (localization length is much greater than $l$), the first term of Eq.(3.26) dominates at $\mathcal{R} \gg \varkappa^{-1}$ and confines the field within the $k_{\max}^{-1}$ -wide layer around the dielectric sheet. However, in the kernel of the local state, within the distance $\mathcal{R} \lesssim \varkappa^{-1}$ from the defect, next terms of Eq.(3.26) begin to compete with the first one. This leads to the $z$-deconfinement of the field inside the kernel. Upon increase of the defect strength, the local state moves away from $\Omega_{\max}$ and the localization length, $\varkappa^{-1}$,decreases. When we are reaching $\overline{\alpha}_{\mathrm{cr}} \sim \omega_1/k_{\max}$, the first term of Eq.(3.26) is no longer dominating in $E(z,\mathbf{r})$. In this case, despite the localization of the field within the $l$-range in radial directions, its $z$ -confinement completely disappears. Such a state can be qualified as a localized waveguide mode. In the waveguide with $l \sim \beta^{-2/3}a$, as we discussed in Chapter 3.1, one can achieve $k_{\max} \sim \omega_1$. In this case the localized modes can be provided by a defect with $\overline{\alpha} \sim 1$, such as an isotope impurity or a local structural defect.

# 4. Summary and Conclusions

In this thesis we investigated the impurity-induced local states in polar crystals. We showed that, in the isotropic approximation, these states arise at the bottom of the polariton gap for infinitesimally small values of the impurity strength. The spectral range available for the local states is extended from the top of the lower polariton band, $\Omega^2_{\max} = \Omega^2_0 - \Delta_1$, to the bottom of the longitudinal phonon band, $\Omega^2_{\min} = \Omega^2_0 + d^2 - \Delta_{\|}$. Our analysis shows that the states near $\Omega^2_{\max}$ are predominated by the long-wavelength polaritons. The typical momentum of these polaritons, $k_{\max}$,defines the coherence length of the local states, $l_{\text{coh}} \sim a\beta^{-1/2}$. The separation of these states from the bottom of the gap, $\sqrt{\omega^2 - \Omega^2_{\max}}$,defines their localization radius, $l_{\text{loc}} \sim a\alpha^{-1}\Omega^2_0\beta^{-1/2}$. Despite an atomic size of a defect, both characteristic lengths are macroscopic.

Since $l_{\text{loc}}$ greatly exceeds $l_{\text{coh}}$, the local states can provide different regimes of the "in-gap" transmission, dependent on the impurity concentration, $n$. When $n^{-1/3} \ll l_{\text{loc}}$ the probability of the tunneling of excitations from one impurity to another is exponentially small, what corresponds to the localized regime. For $l_{\text{coh}} < n^{-1/3} < l_{\text{loc}}$ the resonant tunnelling between impurities gives rise to the diffuse propagation of the radiation. When $n^{-1/3}$ becomes comparable with $l_{\text{coh}}$, the polariton-impurity band begins to form, and the transmission regains properties of the coherent propagation.

The local states drift away from the bottom of the gap upon increase of the impurity strength. This weakens the photon content of the polariton states and transforms them into the ordinary phonon local states. Our estimates of the energy partition, $W_{\text{field}}/W_{\text{mech}} \sim \beta^2$, shows that the local states are phonon-dominated even in the immediate vicinity of the bottom of the gap. The long-wavelength nature of

these states allowed us to analyze the crossover between the polariton and phonon local states within the continuum approximation. Our results demonstrate that the crossover takes place in the narrow interval, $\Delta_1 \sim \beta\ \Omega_0^2$, near the bottom of the gap. However, despite the small size of the crossover interval, the polariton resonance affects the selection of defects allowing local states in the entire gap. In the "narrow" gaps, such that $d^2 - \Delta_{\|} \leq (\Delta_{\|}\,/\,8)\,(2 - \Delta_{\perp}/\Delta_{\|})^2$, there must be only light impurities in the case of the isotope defects.

We analyzed the effects of the impurity-induced variations of the elastic constants on the polariton local states in the cubic crystals. Solving the microscopic equations of motion in the long-wavelength limit, we found two series of the local states of the different parity. The even states resembles the ones considered within the continuum approximation. Their frequencies depend on both parameters, the deviation of the mass, $\delta\mu$, and deviation of the elastic constant, $\delta\nu$. Contrary, the odd states depends on $\delta\nu$ only. These states correspond to the "rhombic" and "tetragonal" oscillations localized around the stationary impurity. Among them the "rhombic" states have the smallest separation from the bottom of the gap, what might indicate the dynamical structural instability of impure cubic crystals.

The features of the polariton local states, in particular the absence of the lower threshold for the impurity strength, are caused by the singularity of the density of states in the lower polariton band, $\rho_-\,(\omega^2) \propto (\Omega_{\max}^2 - \omega^2)^{-1/2}$. This singularity is associated with the long-wavelength polaritons and is generic for any isotropic dipole-active phonon mode with the negative dispersion. We showed that a weak crystal anisotropy removes the singularity from the bottom of the gap, $\rho_-\,(\omega^2) \propto (\Omega_{\max}^2 - \omega^2 + A)^{-1/2}$, and sets a finite threshold for the local states, $\alpha_{\min} \sim \chi^{1/2}\,\Omega_0^2$.

A small width of the crossover region and a suppression of the field component of the local states are the results of a strong difference between the phonon velocity and the speed of light. This disproportion can be eliminated if the active medium is placed inside a waveguide, where the activationless modes are suppressed. We considered an atomically thin dielectric layer ( ionic 2D-crystal ) in a narrow parallel-plate waveguide. The coherent interaction between the waveguide modes and the polarization waves produces new excitations - 2D-polaritons. The structural stability of the 2D-crystal is provided by a strong confining potential, which also eliminates the activationless mode from the 2D-polariton spectrum. In such a system the position of the maximum in the lower polariton branch depends on the waveguide width, $l$. Our analysis shows that $k_{\max} \sim k_0$ when $l \gtrsim \beta^{-2/3}\, a$, and $k_{\max}$ tends to $\beta^{2/3}\, a^{-1}$ for $l \gg \beta^{-2/3}\, a$. In the latter case we found that the frequency range of the local polariton states is enlarged by the factor of $\beta^{-1/3} \sim 10^2$,comparing to the 3D-case. Also, due to the contribution from the upper polariton band, the electromagnetic field in these states is "delocalized" across the 2D-crystal within the distance of the order of $l$ from the defect. Upon increase of the impurity strength, the localization length decreases and the contributions to the field from the lower and upper branches begin to compete everywhere in the waveguide. When the localization radius becomes comparable with the waveguide width, the field is no longer confined near the dielectric layer and the polariton local state transforms into the localized waveguide mode. Our estimates of the critical parameter of a defect show that for $l \sim \beta^{-2/3}\, a$ the localized mode can be provided by a single impurity or a local structural defect.

**Figure 1.** Phonon and polariton dispersion curves.

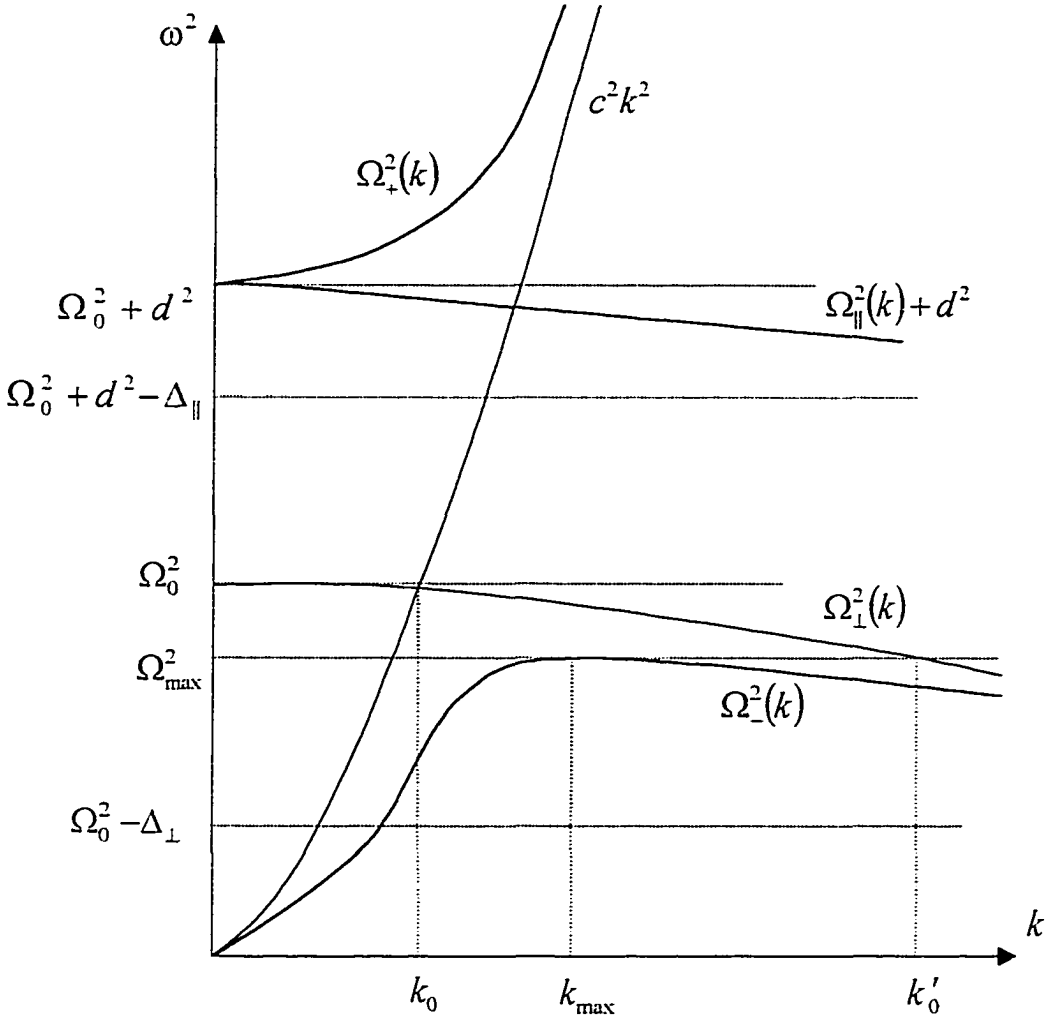


Here $\Omega_\pm$ denote two polariton branches, $\Omega_\perp$ and $\Omega_\parallel$ present transverse and longitudinal phonon branches, $\Omega_0$ is the phonon activation frequency, $\Omega^2_{max} = \Omega^2_0 - \Delta_1$ , $\Delta_\perp$ and $\Delta_\parallel$ denote the widths of the phonon bands, $k_0$ is the cross-resonance momentum, and $k'_0$ is defined by the equation $\Omega_\perp(k'_0) = \Omega_1$ .

**Figure 2.** The elementary cell of the body centered cubic crystal.

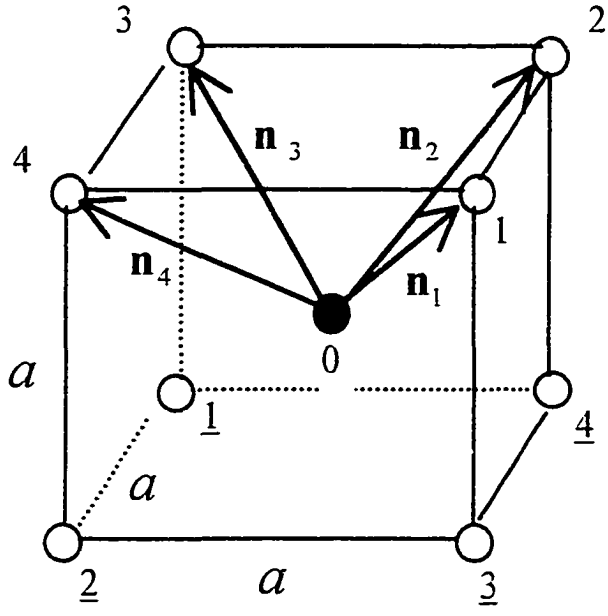


In this picture $a$ is the lattice parameter, and vectors $\mathbf{n}_s$ denote basis vectors

**Figure 3.** 2D-crystal in the parallel-plate waveguide.

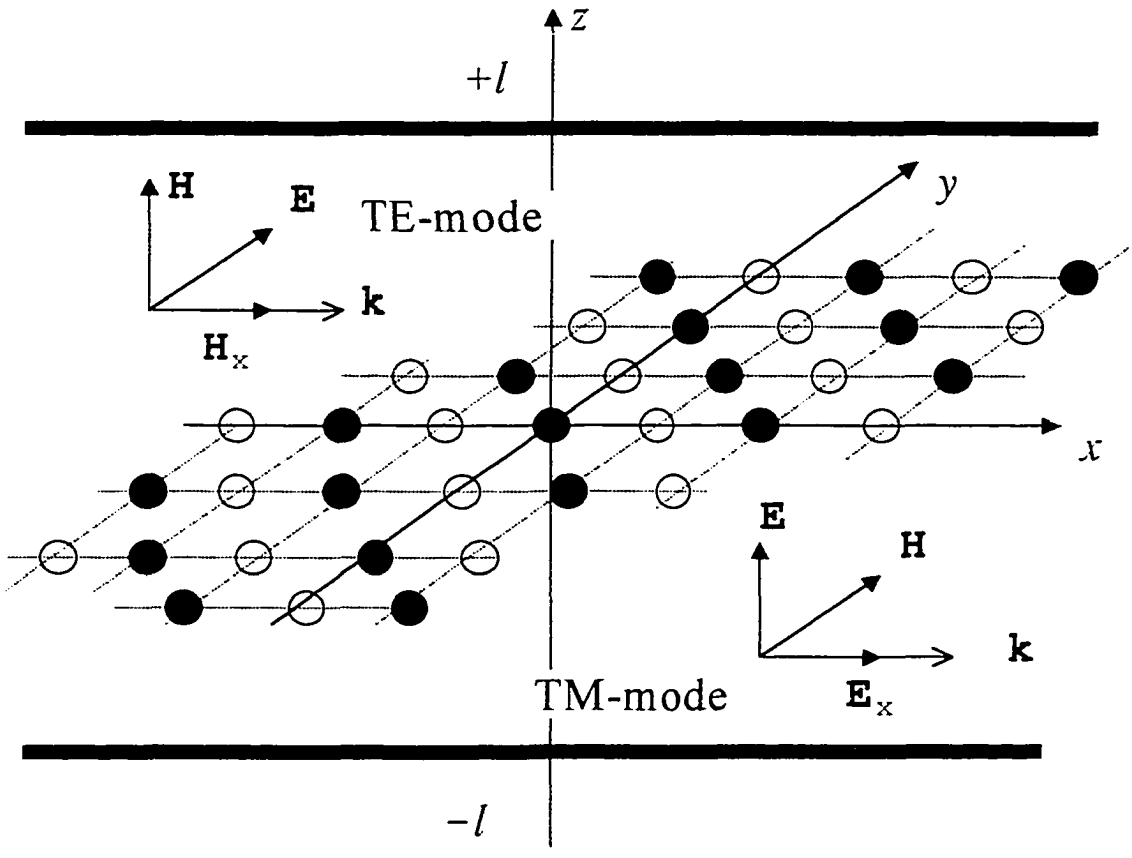


In this picture two horizontal solid bars present the conducting plates, the 2-D crystal is located in the x-y plane and the mutual orientation of **E, H** and **k** in both waveguide modes is shown. The activation frequency of the lattice excitations with the off-plane polarization is assumed to be infinitely large. This, due to the interaction between the lattice and the electromagnetic field, disallows propagation of TM-modes.

**Figure 4.** Graphical solution of the spectral equation (3.3) for $\omega > k$:

$$\frac{\Omega^2 - k^2 - x^2}{k^2 + x^2} = \frac{\delta \tan x}{x}$$

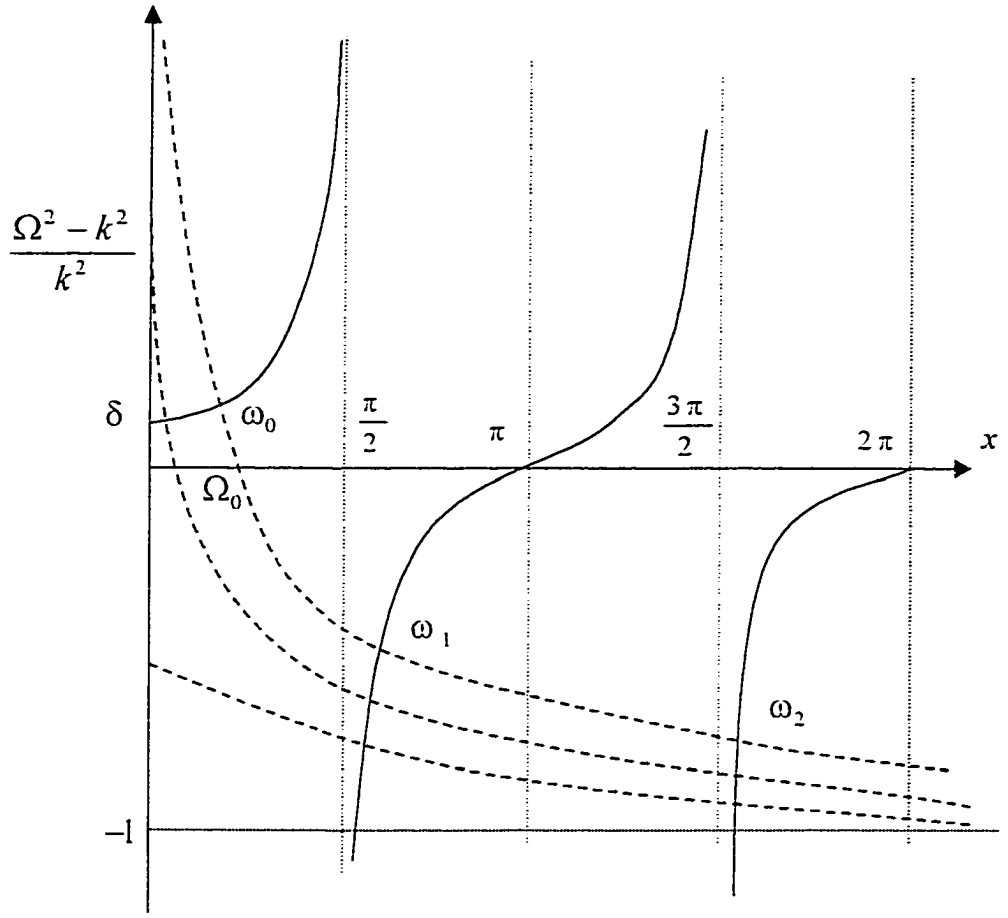


In this picture the solid and dashed lines present the graphs of the functions given by the left-hand and the right-hand sides of the spectral equation. The upper dashed line corresponds to $k=0$, the middle and the lower lines correspond to $k<k_1$ and $k>k_1$, respectively, where $k_1$ is defined by the equation $\Omega^2=k^2(1+\delta)$. The intersections between the solid lines and the upper dashed line define the activation frequencies, $\omega_0, \omega_1, \omega_2, \ldots$ of the corresponding polariton branches, $\omega_0(k)$, $\omega_1(k)$, $\omega_2(k)$,....

**Figure 5.** Graphical solution of the spectral equation (3.3) for $\omega < k$:

$$\frac{\Omega^2 - k^2 + x^2}{k^2 - x^2} = \frac{\delta \tanh x}{x}$$

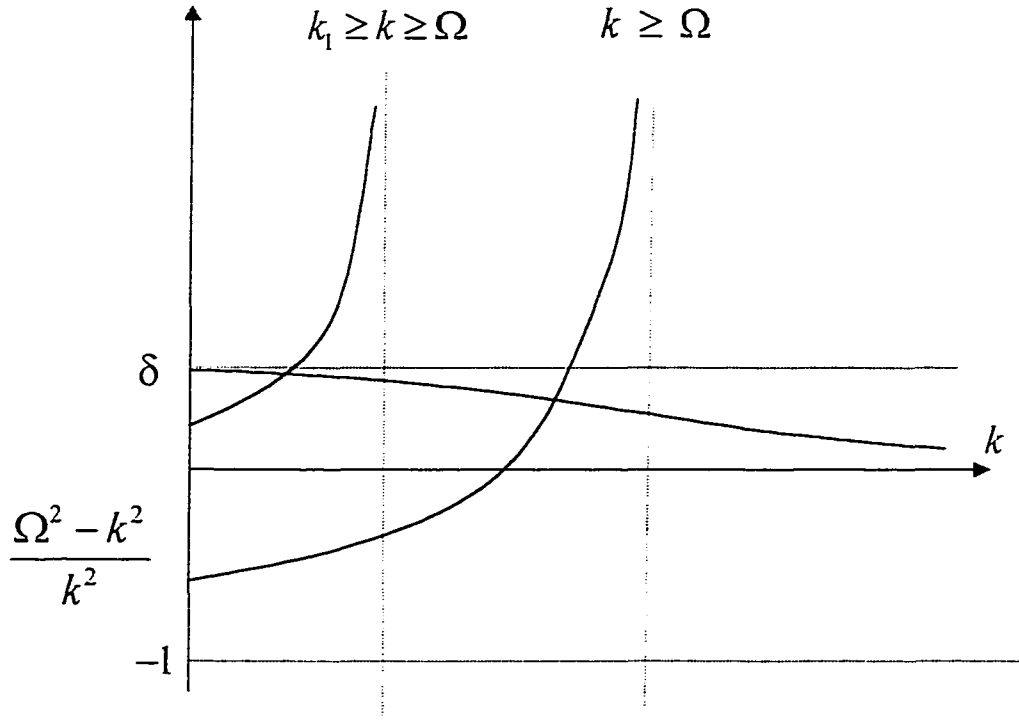


The spectral equation has a unique solution in the region $\Omega^2(k) > (1+\delta)k^2$, where it defines the lower polariton branch $\omega = \omega_0(k)$.

## References


[1] A. Z. Genack, Phys.Rev. Lett. **58**, 2043 (1987),

M. Drake and A. Z. Genack, Phys.Rev. Lett. **63**, 259 (1989).

[2] S. John, Phys. Rev.Lett **53** 2169 (1984), Phys. Rev. B **31** 304 (1985).

[3] *Scattering and localization of classical waves in random media*, edited by Ping Sheng (World Scientific, Singapore, 1990).

[4] B.A. van Tiggelen, A. Lagendijk, M.P. van Albada, and A.Tip, Phys. Rev. B **45**, 12233 (1992).

[5] Yu.N. Barabanenkov and V.D. Ozrin, Phys. Rev. Lett.**69** , 1364 (1992)

[6] K. Arya, Z. B. Su and J. L. Birman, Phys. Rev.Lett **57** 272 (1986),

[7] T. R. Kirkpatrick, Phys. Rev. B **31**, 5746 (1985), C. A. Condat and T. R. Kirkpatrick, Phys. Rev.Lett **58** 226 (1987)

[8] G. Cwilich and Y. Fu, Phys. Rev. B **46**, 12015 (1992).

[9] E. Yablonovich, Phys.Rev.Lett. **58**, 2059 (1987), E. Yablonovich and T. J. Gmitter, Phys.Rev.Lett. **63**, 1950 (1989)

[10] S. John, Phys.Rev.Lett. **58**, 2486 (1987), S. John and R. Rangarajan, Phys.Rev. B **38**, 10101 (1988), S. John and T.Wang, Phys.Rev.Lett. **64**, 2418 (1990), Phys.Rev. B **43**, 12772 (1991).

[11] *Photonic Band Gaps and Localization*, edited by C. M. Soucoulis (Plenum Press, New York, 1993).

[12] V.I. Rupasov and M. Singh, Phys. Rev. Lett. **77**, 338 (1996).

[13] V.I. Rupasov and M. Singh, Phys. Rev. A **56** 898 (1997), S. John and V.I. Rupasov, Phys. Rev. Lett. **79**, 821 (1997).

[14] L.I. Deych and A.A. Lisyansky, Phys. Lett. A, **4**, 340 (1998).

[15] A. A. Maradudin, I. M. Lifshitz, A. M. Kosevich, W. Cochran, and M. J. P. Musgrave, *Lattice Dynamics* (Benjamin, New York. 1969).

[16] A.A. Maradudin, E.W. Montroll, G.H. Weiss, and I.P. Ipatova, *Theory of Lattice Dynamics in the Harmonic Approximation* (Academic Press, New York, 1971).

[17] I. M. Lifshitz, Docl. Acad. Nauk S.S.S.R., **48**, 83 (1945), Zh. Eksp. Teor. Fiz., **17**, 1017 (1947), **18**. 298 (1948).

[18] M. Born and K. Huang, *Dynamical Theory of Crystal Lattices* (Oxford, Clarendon Press, 1954)

[19] V.S. Podolsky, *Crossover between polariton and phonon local states. Anisotropy-induced localization threshold*, e-print/cond-mat/9803375, Phys. Rev. B (to be submitted) .

[20] V.S. Podolsky, L.I. Deych and A.A. Lisyansky, Phys. Rev. B1 **57** 5168 (1998).

[21] V.S. Podolsky, *Polaritons in 2D-crystals and localized modes in narrow waveguides*, e-print/cond-mat/9804074, Phys. Rev. B (to be submitted).

[22] C. Kittel *Introduction to solid state physics* (Willey, New York, 1986).

[23] A.Figotin and A. Klein, Preprint (1997).

# IMAGE EVALUATION TEST TARGET (QA-3)

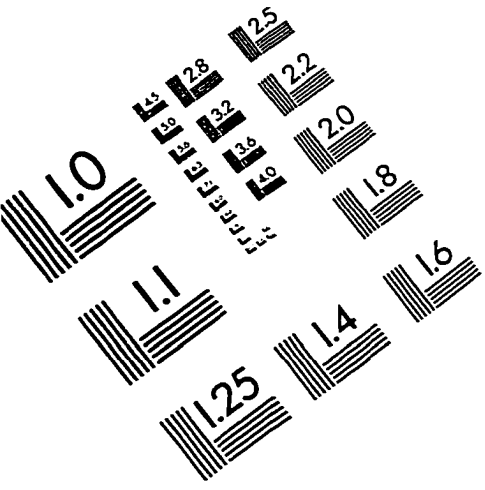


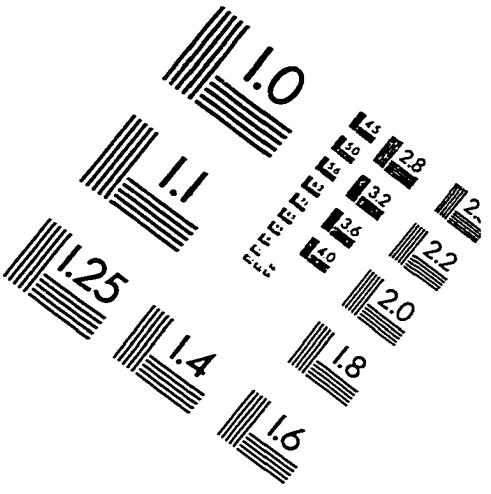


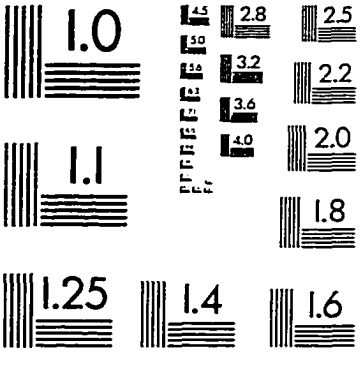


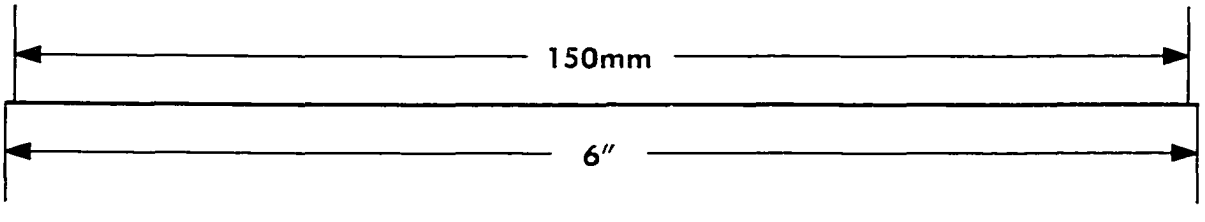


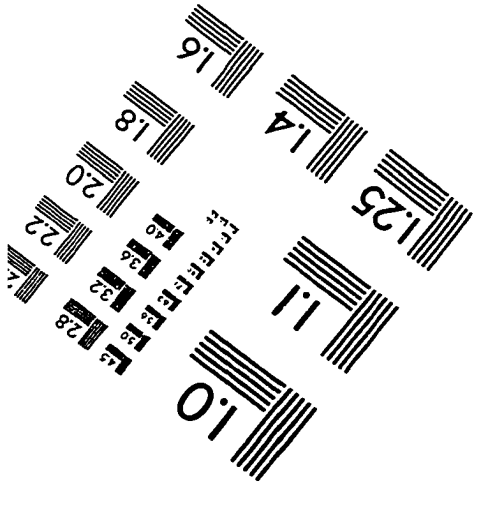


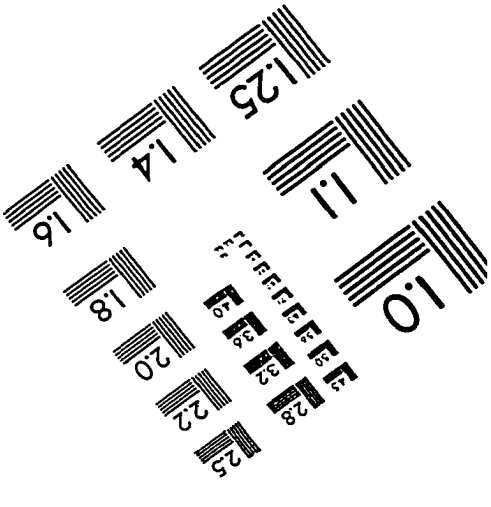


APPLIED IMAGE, Inc
1653 East Main Street
Rochester, NY 14609 USA
Phone: 716/482-0300
Fax: 716/288-5989